Space Sci Rev
DOI 10.1007/s11214-014-0053-7

The Aeronomy of Mars: Characterization by MAVEN of the Upper Atmosphere Reservoir That Regulates Volatile Escape

S.W. Bougher · T.E. Cravens · J. Grebowsky · J. Luhmann

Received: 27 September 2013 / Accepted: 19 May 2014

Abstract The Mars thermosphere-ionosphere-exosphere (TIE) system constitutes the atmospheric reservoir (i.e. available cold and hot planetary neutral and thermal ion species) that regulates present day escape processes from the planet. The characterization of this TIE system, including its spatial and temporal (e.g., solar cycle, seasonal, diurnal, episodic) variability is needed to determine present day escape rates. Without knowledge of the physics and chemistry creating this TIE region and driving its variations, it is not possible to constrain either the short term or long term histories of atmosphere escape from Mars. MAVEN (Mars Atmosphere and Volatile Evolution Mission) will make both in-situ and remote measurements of the state variables of the Martian TIE system. A full characterization of the thermosphere (∼100–250 km) and ionosphere (∼100–400 km) structure (and its variability) will be conducted with the collection of spacecraft in-situ measurements that systematically span most local times and latitudes, over a regular sampling of Mars seasons, and throughout the bottom half of the solar cycle. Such sampling will far surpass that available from existing spacecraft and ground-based datasets. In addition, remote measurements will provide a systematic mapping of the composition and structure of Mars neutral upper atmosphere and coronae (e.g. H, C, N, O), as well as probe lower altitudes. Such a detailed characterization is a necessary first step toward answering MAVEN's three main science questions (see Jakosky et al. 2014, this issue). This information will be used to determine present day escape rates from Mars, and provide an estimate of integrated loss to space throughout Mars history.

S.W. Bougher (✉)
Department of Atmospheric, Oceanic and Space Sciences, University of Michigan, Ann Arbor, MI 48109, USA
e-mail: bougher@umich.edu

T.E. Cravens
Department of Physics & Astronomy, University of Kansas, Lawrence, KS 66045, USA

J. Grebowsky
NASA Goddard Space Flight Center, Greenbelt, MD 20771, USA

J. Luhmann
Space Sciences Laboratory, University of California Berkeley, Berkeley, CA 94720, USA

Published online: 30 August 2014

Keywords Mars · Aeronomy · Thermosphere · Ionosphere · MAVEN Mission

1 Motivation

1.1 Why Mars Aeronomy Is Key to MAVEN Mission Goals

The term 'aeronomy' is attributed to an interdisciplinary field that studies the physics and chemistry of any atmospheric region where ionization and photo-dissociation processes play a key role (e.g. Chapman 1931). In this formulation, aeronomy is applicable to the entire Martian atmosphere, including the upper, middle and lower atmospheres, since photo-dissociation is important throughout. However, the upper atmospheric region includes the planetary thermosphere, ionosphere and exosphere (also sometimes referred to as the corona). They are key to understanding how energy and material flow into and out of the main atmosphere- the latter of which includes the escaping component that is so important to the goals of the MAVEN mission to Mars (see Jakosky et al. 2014 and other papers in this issue). These atmosphere regions are also important for understanding the Martian ionosphere that, together with Mars crustal magnetic fields, provides the obstacle to the solar wind interaction. In addition, the neutral atmospheric regime (thermosphere) also controls spacecraft orbital dynamics and aerobraking maneuvers. Overall, the Martian upper atmosphere is the conduit linking the external environment and the surface and main atmosphere. This key region needs to be understood in order to elucidate the atmospheric escape processes.

1.2 What Are the Basic Features, Processes and Vertical Extent of This Upper Atmosphere Reservoir?

The Mars dayside thermosphere (∼100–200 km) is commonly characterized by temperatures that increase dramatically with altitude above the mesopause (located at ∼90–110 km), largely due to solar EUV-UV heating, while approaching an asymptotic and maximum value at an altitude of ∼160–200 km. It is distinguished by a transition region called the homopause (located at ∼125 km mean altitude on the dayside), below which atomic and molecular constituents are well mixed by winds and dissipative turbulence (e.g. Stewart 1987; Bougher 1995; Bougher et al. 2000, 2009a, 2009b, 2014). Above the homopause region, is the heterosphere, where individual species begin to separate according to their unique masses and scale heights via atomic/molecular diffusion. Mars' thermosphere is dominated by CO_2 and its dissociation products O and CO, as well as N_2. The thermospheric layer extends from the top of the middle atmosphere (mesopause) to the beginning of collision-free space (exobase). Most importantly, the thermosphere is an intermediate atmospheric region (see Fig. 1) strongly coupled to the lower-middle atmosphere (e.g. seasonal inflation/contraction, gravity waves, planetary waves, thermal tides, dust storms) and also coupled from above with energy inputs from the Sun (solar X-ray, EUV, and UV fluxes, and solar wind particles) (see reviews by Bougher 1995; Bougher et al. 2002, 2009a, 2009b, 2014).

Since Mars presently has a very small intrinsic magnetic field, consisting of localized near surface remnant field regions, the solar EUV, UV and near-IR heating are the primary (periodic) drivers of the Mars thermospheric thermal structure (e.g. Bougher 1995; Bougher et al. 2000, 2009a, 2009b, 2014). However, the solar wind impact on Mars is not isolated to localized regions. This Mars situation is unlike the Earth, where the field structure leads

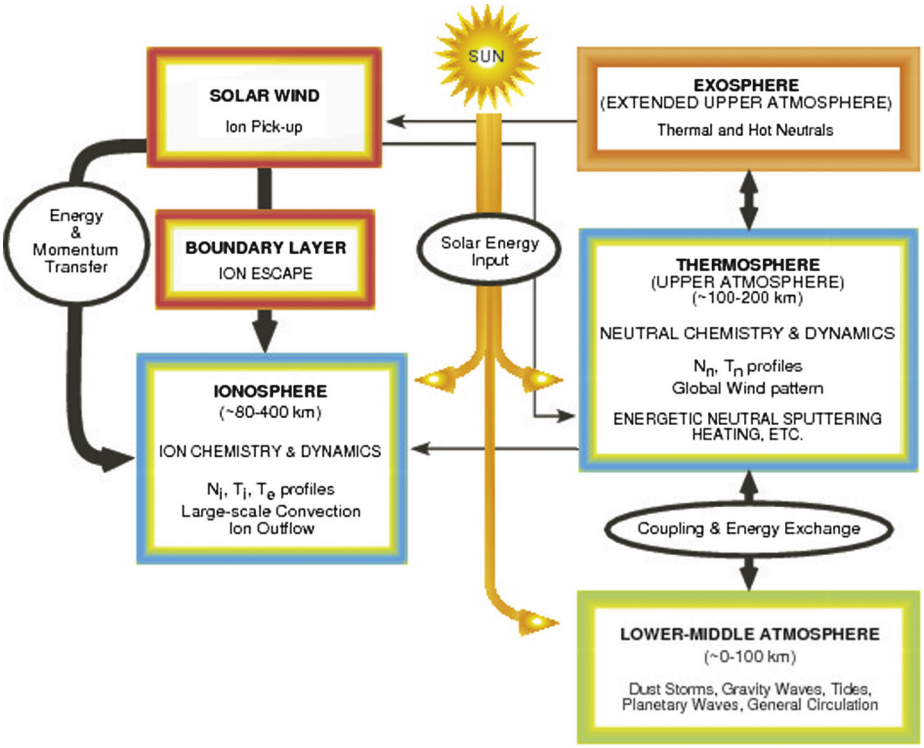

Fig. 1 Cartoon of Mars atmospheric regions and processes. Illustrates the coupling of the thermosphere and ionosphere with atmospheric regions above and below

to large inputs of solar wind generated energy inputs focused at auroral latitudes, resulting in large changes in the atmosphere. The radiative heat deposited at Mars is conducted downward toward the mesopause by molecular thermal conduction, where it is partially radiated away to space by CO_2 15-micron emission. Global scale winds transport atomic and molecular constituents around the planet, as well as dayside produced heat, giving rise to an intricate feedback of global composition, temperature, and wind fields (see Bougher et al. 1999a, 1999b, 2000, 2006, 2009a, 2009b).

The primary charged particles (e.g. O_2^+, CO_2^+, O^+, N_2^+, CO^+, NO^+, etc.) that make up the Mars ionosphere (a weakly ionized plasma embedded within the thermosphere) are formed by: (1) solar EUV fluxes and their generation of photo-electrons that ionize local neutral thermospheric species (e.g. CO_2, N_2, CO, O, etc.); (2) precipitating particles (e.g. suprathermal electrons) that ionize these same neutral species (especially on the nightside); and (3) ion-neutral photochemical reactions (e.g. Fox 2009; Bougher et al. 2014). The solar zenith angle (SZA) dependence of the dayside neutral thermospheric structure is directly reflected in the ionospheric structure (see reviews of Withers 2009; Haider et al. 2011). Since Mars lacks a significant intrinsic global magnetic field, the variable solar wind (including its particles, the interplanetary magnetic field, and the solar wind convection E field) penetrates and interacts with the Mars upper atmosphere (including the thermosphere, ionosphere and exosphere). This results in additional ionization, and various types of ion energization and neutral heating (see Lillis et al. 2014). Detailed reviews of the solar wind interaction can be found in Chassefiere and Leblanc (2004) and Brain et al. (2014).

The Mars upper atmosphere can change dramatically over time since this atmospheric region is primarily controlled by two highly variable components of the Sun's energy output composed of solar radiation (0.1–200 nm) and the solar wind (see reviews by Bougher et al. 2002, 2009a, 2009b, 2014). The amount of the soft X-ray (0.1–5 nm) and EUV (5–110 nm) solar radiation most responsible for heating the Mars thermosphere (and forming its ionosphere) varies significantly over time (e.g. see Eparvier et al. 2014). These temporal variations result from Mars' changing heliocentric distance as it orbits the Sun (∼1.38–1.67 AU), the planet's obliquity (determining the local season), and the short-term changes in the radiation from the Sun itself. It is noteworthy that solar EUV-UV fluxes received at Mars vary by 44 % throughout the Martian year, solely the result of the changing heliocentric distance. Both solar rotation (∼27-day) and solar cycle (∼11-year) variations of the solar EUV and soft X-ray fluxes are also significant (up to factors of ∼ 3 to 100), producing dramatic variations in global thermospheric temperatures, composition, and winds (e.g. Bougher et al. 2000, 2002, 2009a, 2009b; Forbes et al. 2008), as well as ionospheric densities (e.g. Fox et al. 1996; Withers 2009; Haider et al. 2011).

Above the thermosphere, in the exosphere, collisions no longer dominate and the lightest species form an extended hot corona, some of which escapes to space (see exosphere discussion below) (e.g. Valeille et al. 2009a, 2009b, 2010a, 2010b; Yagi et al. 2012; Lee et al. 2014). Mars with its weak gravity (unlike Venus and Earth) permits an extended corona of several species (e.g. O, N, C, H). The "traditionally labeled" boundary between the thermosphere and exosphere is the exobase, defined as the level above which an escaping particle moving along a radial direction will encounter only one collision on average (e.g. Valeille et al. 2009a, 2009b; Schunk and Nagy 2009). For a single constituent upper atmosphere, this is equivalent to the altitude where the collision mean free path equals the temperature scale height of the constituent (e.g. Schunk and Nagy 2009). More recently, it has become understood that the transition from the collisionally dominated thermosphere (below ∼200 km) to the kinetic dominated extended exosphere (above ∼300 km) is not a sharp boundary (e.g. Valeille et al. 2009a, 2009b, 2010a, 2010b; Fox and Hać 2009, 2010).

The exosphere is also populated by 'nonthermal' species related to the ionospheric photochemistry of the CO_2 atmosphere. For example, dissociative recombination of the primary O_2^+ ion, as well as other minor constituents such as CO^+, produce important enhancements to the thermal exosphere species O and C. In particular, approximately half of the hot O produced by the exothermic dissociative recombination of O_2^+ with electrons can escape, which makes characterizing this process, and understanding the ionosphere, an essential task for MAVEN. In addition, charge exchange between the exospheric thermal H and solar wind protons can produce a non-thermal H component (although at the expense of the thermal exospheric H). An understanding of the Martian exosphere is important for quantifying atmospheric ion and neutral escape rates, needed in particular for estimating the global loss of water over Mars history (e.g. Chassefiere and Leblanc 2004; Valeille et al. 2009b).

Transient solar events compete with the periodic solar variations (i.e. diurnal, seasonal, solar cycle) in controlling thermospheric heating. In addition, Mars surface events (such as major dust storms) can temporarily alter its atmospheric global responses to solar radiation. It is noteworthy that episodic heating of the Mars thermosphere is expected, yet still unconfirmed, by enhancements in the EUV flux and solar wind changes due to solar flares. Coronal Mass Ejection (CME) events, and various solar wind interaction processes may also significantly modify the normal periodic (solar driven) thermospheric structure. Alternatively, dust storms change the atmosphere's opacity, resulting in lower atmosphere aerosol heating and expansion of the entire atmosphere. Upward propagating planetary atmosphere

waves and tides can also have a significant influence on thermospheric structure and dynamics (e.g. Forbes and Hagan 2000; Forbes et al. 2002; Wilson 2002; Withers et al. 2003; Moudden and Forbes 2008; Bougher et al. 2014). Limited measurements suggest that this influence is felt most strongly in the thermosphere when regular solar forcing is at a minimum (e.g. Seiff and Kirk 1977). And, of course the ionosphere responds to changes in the neutral atmosphere structure (e.g. Bougher et al. 2004, 2014).

The Mars TIE system constitutes the atmospheric reservoir (i.e. available cold and hot planetary neutral and thermal ion species) that regulates present day escape processes from the planet (see Brain et al. 2014). The characterization of this TIE system, including its spatial and temporal (e.g., solar cycle, seasonal, diurnal) variability is needed to determine the escape rates. For example, the Mars thermosphere regulates the escape by: (1) absorbing and spatially redistributing solar EUV and UV energy, (2) filtering and absorbing upward propagating waves of various scales, (3) mediating interactions between the solar wind and the ionosphere, and (4) controlling the upward transport of species from the lower atmosphere through diffusion and large-scale dynamics to where they can be removed (see Bougher et al. 2014). As discussed further below, it is within this region that either sufficient energy is imparted to constituents to allow either direct escape as neutrals or ions, or indirect escape by exposing them to removal agents such as the solar wind and its related electric and magnetic fields. Without knowledge of the physics and chemistry creating this TIE region and driving its variations, it is not possible to constrain either the short term or long-term histories of atmosphere escape.

The interconnectedness of Martian volatile escape processes and the underlying TIE reservoir are now being investigated (and appreciated) through specific model simulations that link its regions and processes. Recent numerical experiments that couple global thermosphere-ionosphere and exosphere codes (see Lillis et al. 2014) strongly suggest that seasonal, plus solar cycle variations of the thermosphere-ionosphere structure have a profound impact upon computed hot O and C distributions and the corresponding hot atom escape rates (see Valeille et al. 2009a, 2009b; Yagi et al. 2012; Lee et al. 2014). Likewise, the solar cycle plus seasonal variations in the combined TIE system are predicted to have a profound impact on variations in the sources of ions, the extended ionosphere structure and the resulting ion escape rates (see Ma and Nagy 2007; Lundin et al. 2008; Najib et al. 2011; Dong et al. 2014). In short, each of the present day neutral and ion escape mechanisms is regulated to some degree by the changing solar EUV radiation and the resulting variation in the TIE structure (see reviews of Bougher et al. 2014 and Brain et al. 2014). However, a comprehensive observational study that characterizes the Martian TIE reservoir related to escape processes has yet to be realized.

In this paper we specifically focus on measurements that the MAVEN mission will be providing to expand our knowledge of the upper atmosphere (i.e. TIE system) and its drivers and variability. In addition, we outline several outstanding questions about the Martin upper atmosphere that MAVEN measurements are designed to address. The aim is to provide the reader with a sense of the level of global observational coverage and detailed information that will become available in the area of Mars aeronomy, and an understanding of how all of this information will inform investigations and models of atmospheric escape and evolution, the mission's main goal.

The MAVEN mission (see Jakosky et al. 2014) is slated to make systematic measurements that will characterize the TIE reservoir. MAVEN's three main science objectives cannot be addressed without starting with the first, which is the focus of this paper; i.e. to determine the composition, structure, and dynamics of the upper atmosphere and the processes controlling them.

2 Major Unanswered Questions about the Martian Upper Atmosphere

The MAVEN mission is designed to obtain key measurements that will be used to address several outstanding problems, thereby enhancing our understanding of the climatology and variability of the Martian upper atmosphere structure and the processes that control them. This section reviews these major questions. Section 3 will discuss the corresponding MAVEN measurements to be obtained and their application to these problems.

2.1 Thermosphere

2.1.1 What Are the Global Thermosphere and Exosphere Temperature Structures and How Do These Vary Both Spatially and Temporally?

Presently, the Martian upper atmosphere thermal structure is poorly constrained by a limited number of both in-situ and remote sensing measurements at selected locations, seasons, and periods scattered throughout the solar cycle (see reviews by Stewart 1987; Bougher 1995; Bougher et al. 2000, 2014; Müeller-Wodarg et al. 2008). In particular, the vertical thermal structure of the upper atmosphere has been sampled many times, but only in limited latitude/local time zones, and mostly during solar minimum to moderate conditions (see review by Bougher et al. 2014). Existing temperature profiles include those from: (a) Viking Landers 1 and 2 entry accelerometers on the dayside based on mass density scale heights (Seiff and Kirk 1977), (b) Viking Landers 1 and 2 Upper Atmosphere Mass Spectrometer (UAMS) on the dayside (Nier and McElroy 1977), (c) Mars Global Surveyor (MGS), Mars Odyssey (MO), and Mars Reconnaissance Orbiter (MRO) aerobraking accelerometers for both dayside and nightside (e.g., Keating et al. 1998, 2003, 2006, 2008), and (d) Mars Express SPICAM (mostly nightside) inferred from stellar occultations (Forget et al. 2009; McDunn et al. 2010). In addition, vertical profiles of key dayglow emissions observed by Mariners 6, 7, 9, and Mars Express have been used to extract temperatures, especially topside (exosphere) values (e.g. Stewart 1972; Stewart et al. 1972; Leblanc et al. 2006; Huestis et al. 2010; Stiepen et al. 2014). Generally, dayside isothermal temperatures are found above ∼160 km for solar minimum conditions, and at higher altitudes for solar moderate-to-maximum conditions (e.g. Keating et al. 2008; Bougher et al. 2014).

The Mars orbit eccentricity demands that both the solar cycle and seasonal variations in upper atmosphere temperatures be considered together (e.g., Bougher et al. 2000). These combined variations in Martian dayside upper thermosphere and exosphere temperatures have been the subject of considerable debate and study since the first Mariner 6, 7, and 9 ultraviolet spectrometer (UVS) measurements (1969–1972), up to recent Mars Express SPICAM UVS measurements (2004–present) (e.g., Stewart 1987; Bougher et al. 1999b, 2000, 2009b, 2014; Keating et al. 2003, 2008; Withers 2006; Leblanc et al. 2006; Forbes et al. 2008; González-Galindo et al. 2009; Krasnopolsky 2010; Huestis et al. 2010; Stiepen et al. 2014). Presently, a "composite estimate" exists of the extreme solar cycle plus seasonal variation of Martian dayside exospheric temperatures, from ∼200 K to ∼350 K (see Bougher et al. 2014). However, this estimate is most uncertain for solar moderate-to-maximum conditions, for which little data is available (see Fig. 2). It is noteworthy that this "composite" range of Mars exospheric temperatures is likely larger than that of Venus (see reviews of Bougher 1995; Bougher et al. 1997; Kasprzak et al. 1997). Finally, lower atmosphere influences upon upper atmosphere temperature variations are only beginning to be characterized (e.g. Stiepen et al. 2014).

A full characterization of the thermospheric temperature structure (∼100–250 km) requires spacecraft measurements that systematically span all local times and latitudes, over

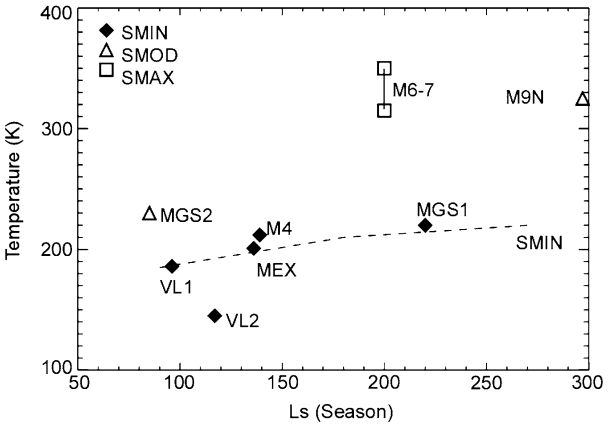

Fig. 2 Mars dayside (low SZA) exospheric temperatures from previous spacecraft measurements obtained at different Mars seasons and periods during the solar cycle. Symbols are as follows: *diamonds* (SMIN conditions, F10.7 ∼ 70), *triangles* (SMOD conditions, F10.7 ∼ 130), and *squares* (SMAX conditions, F10.7 ∼ 200). Superimposed SMIN thermosphere simulation results are added to illustrate the predicted role of seasonal forcing. Spacecraft abbreviations are as follows: VL1 (Viking Lander 1), VL2 (Viking Lander 2), M4 (Mariner 4), MEX (Mars Express), MGS1 (MGS Phase 1 Aerobraking), MGS2 (MGS Phase 2 Aerobraking), M9N (Mariner 9 nominal mission), M6-7 (Mariner 6-7). *Adapted from Bougher et al.* (2000), *Fig. 2. J. Geophys. Res*., *American Geophysical Union*

a regular sampling of Mars seasons, and throughout the solar cycle. Such temperature measurements of the topside thermosphere and into the exosphere (above ∼150 km) would be most important for constraining escape model simulations and determining volatile escape rates. Sections 3.1.1 (NGIMS) and 3.2.1 (IUVS) contain a discussion of MAVEN measurements that will be made to constrain these neutral thermospheric temperatures.

2.1.2 What Are the Neutral Species (Especially Atomic Oxygen) Global Density Distributions and How Do These Vary Both Spatially and Temporally?

The composition of the Mars thermosphere, specifically neutral species densities, has thus far only been directly measured with the UAMS instruments onboard the descending Viking 1 and 2 Landers (e.g., Nier and McElroy 1977). The two sets of density profiles, corresponding to solar minimum near aphelion conditions, reveal CO_2 to be the major species, followed by N_2 and CO (see Fig. 3). Atomic O could not be measured by the UAMS; instead, ionosphere model calculations (to match the Viking Lander 1 ion composition measurements) have estimated that the O density exceeds the CO_2 density at ∼200 km (e.g., Hanson et al. 1977). This uncertain abundance of O is a major unknown for the Mars upper atmosphere; in particular, systematic measurements of atomic O (both spatially and temporally) are needed to constrain the heat budget and chemistry of the dayside thermosphere (see review by Bougher et al. 2014). Systematic neutral density measurements (both dayside and nightside) are also essential for characterizing the target atmosphere that is ionized (or sputtered), providing the major sources for neutral and ion escape.

The study and inversion of airglow emissions can also be used at Earth and other planets to retrieve neutral densities and temperatures. Specifically, detailed Martian studies have been conducted for example to extract O and CO_2 density profiles from key dayglow emissions from Mariner and Mars Express datasets (e.g. Strickland et al. 1972, 1973; Stewart et al. 1992; Chaufray et al. 2009; Gronoff et al. 2012). Retrieval techniques utilized for

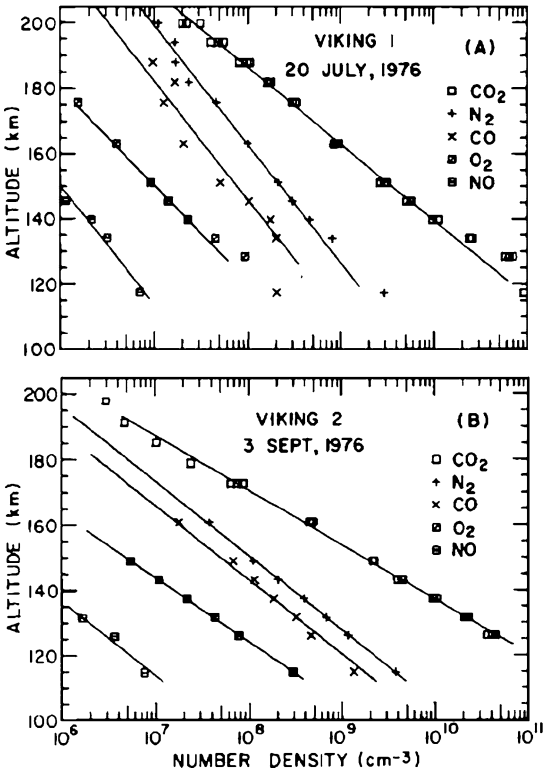

Fig. 3 Number densities of CO_2, N_2, CO, O_2, and NO determined from measurements made by upper atmospheric mass spectrometers (UAMS) on the Viking 1 and 2 Landers. Ar was also measured but is not shown here. *Taken from Nier and McElroy* (1977)*, Fig. 4. J. Geophys. Res., American Geophysical Union*

these Mars investigations are constantly being improved. However, density retrievals are limited owing to sampling conditions available from existing (and limited) datasets. Alternatively, a spectrum obtained from FUSE measurements is of superior quality and resolution (Krasnopolsky and Feldman 2002), yet it has not been studied in detail to extract the densities of the Martian thermosphere and ionosphere.

On the other hand, mass densities of the Mars thermosphere (between ∼100 and ∼160 km) have been repeatedly measured by accelerometers onboard MGS, MO, and MRO spacecraft (e.g., Keating et al. 1998, 2003, 2006, 2008; Bougher et al. 1999a, 2006, 2014; Tolson et al. 1999, 2005, 2007, 2008; Withers et al. 2003; Withers 2006). The accelerometer sampling occurred at limited seasons and solar cycle conditions, as well as restricted (latitude, local time) locations dictated by their spacecraft orbits (see Fig. 4). A strong variation of mass densities with latitude was observed, along with distinct differences in the polar night regions between the aphelion and perihelion seasons. The accelerometer samplings of mass densities provide the best existing record of Mars' upper atmosphere structure, much more extensive than the two Viking descent profile measurements of neutral densities (see review by Bougher et al. 2014). However, by its nature, accelerometer spatial and temporal coverage is quite sparse, providing only a rudimentary database for characterizing the upper atmosphere structure and its variations over the solar cycle and Mars seasons.

A full characterization of Martian thermospheric composition (∼100–250 km) requires spacecraft measurements that systematically span all local times and latitudes, over a regular sampling of Mars seasons, and throughout the solar cycle. Sections 3.1.1 (NGIMS) and 3.2.1 (IUVS) provide a discussion of MAVEN measurements that will be made to constrain neutral thermospheric densities, especially atomic O. In addition, the Accelerome-

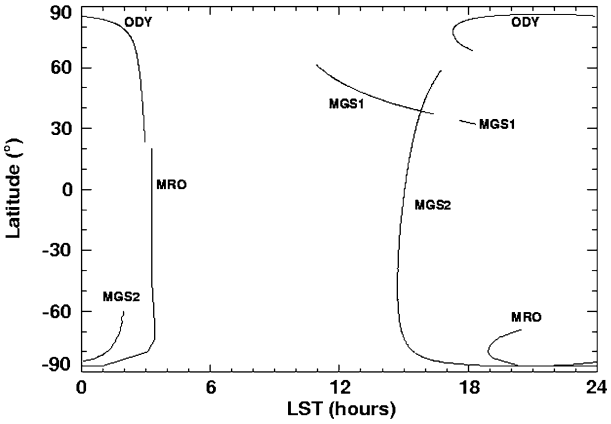

Fig. 4 US Accelerometer coverage for MGS (two phases), Odyssey, and MRO aerobraking campaigns. Periapsis locations for each orbit as a function of latitude and local time. *Adapted from Tolson et al.* (2007), *Fig. 1c. Journal of Spacecraft and Rockets*

ter Experiment (ACC) will also use atmospheric drag accelerations sensed by the Inertial Measurement Units (IMU) onboard the spacecraft to recover atmospheric density (and derive corresponding neutral temperatures) which can also be used to constrain thermospheric structure (see Zurek et al. 2014, this issue).

2.1.3 How Does the Thermospheric Structure Respond to Lower Atmosphere Forcing (e.g. Upward Propagating Waves and Dust Storms)?

Presently, mass densities derived from accelerometer measurements reveal large-amplitude Sun-synchronous longitudinal variations at altitudes of ∼100–160 km (e.g., Keating et al. 1998; Forbes and Hagan 2000; Forbes et al. 2002; Withers et al. 2003; Bougher et al. 2014). They generally appear as stationary waves from an orbit that precesses slowly in local time (e.g., Forbes and Hagan 2000; Forbes et al. 2002; Wilson 2002; Angelats i Coll et al. 2004; Moudden and Forbes 2008, 2010) and are likely produced by vertically-propagating non-migrating solar thermal tides that are excited near Mars' surface and propagate into the thermosphere. However latitude/local time (spatial) and seasonal (temporal) sampling of these longitude features is sparse (see Fig. 4). Excitation of these waves is commonly attributed to topographic modulation of near-surface solar heating (e.g., Forbes et al. 2002). However, secondary contributors to the excitation of these non-migrating tides are also being investigated (Moudden and Forbes 2008, 2010). The neutral thermospheric waves are also observed to have a corresponding impact on the ionosphere structure; e.g., the height of the main ionospheric peak varies in step with these longitude features (e.g. Bougher et al. 2004, 2014; Withers 2009; Haider et al. 2011).

Dust storm impacts on the upper atmosphere are only beginning to be observed and understood (see reviews by England and Lillis 2012; Withers and Pratt 2013). The Noachis regional dust storm of 1997–1998 occurred during MGS aerobraking, providing a striking picture of the significant blooming (factor of three enhancement) of upper atmospheric densities (at a constant altitude) during the onset of the storm (e.g. Keating et al. 1998; Bougher et al. 1999a, 2014). See Fig. 5. Subsequent dust storm events (e.g. July 2005) did not have upper atmosphere sampling with accelerometers. However, ∼4 Martian years of MGS electron reflectometry (ER) data were recently employed to derive neutral mass densities at ∼185 km on the nightside near 2 AM local time (Lillis et al. 2010). Seasonally repeating features included: (a) overall expansion/contraction of the nighttime thermosphere with heliocentric distance, and (b) much lower densities at the aphelion winter pole compared to

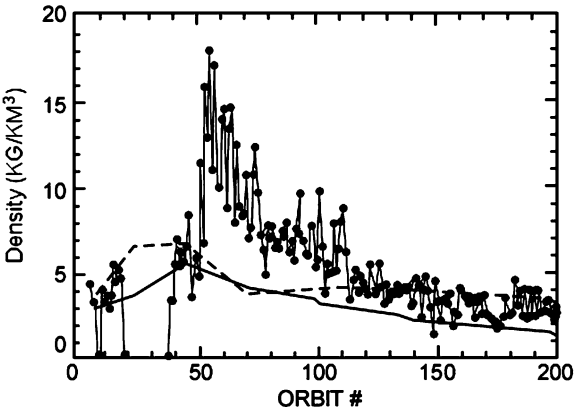

Fig. 5 Noachis dust storm evolution of mass densities at 130 km obtained by the MGS Accelerometer Experiment (ACC). Orbits ∼10–200 are displayed, spanning Ls ∼ 188–300 (28-September 1997 to 27-March 1998) corresponding to pre-storm (#10–49), plus Noachis storm onset and its gradual decay (#50–200). The Noachis storm started at Ls ∼ 224 (27-November 1997). Superimposed MTGCM simulations correspond to static dust cases (tau = 0.3, *solid curve*; tau = 1.0, *dashed curve*). *Adapted from Bougher et al.* (1999a), *Fig. 2. Adv. Space Research*

the perihelion winter pole. In addition, inter-annual differences were observed, and may be related to changing dust opacities.

A vastly improved characterization of Martian upper atmosphere responses to lower atmosphere forcing (e.g. waves and dust storms) requires spacecraft measurements that systematically span all local times and latitudes, over a regular sampling of Mars seasons. This would remove the aliasing problem encountered with tidal analyses, which thus far have utilized only two local time sampling (over most latitudes) provided by most orbiter missions. One notable exception to this aliasing problem is provided by MRO/MCS off axis sampling that provided an opportunity to sample at several local times, thereby confirming the usefulness of such observations for conducting detailed tidal analyses (e.g. Lee et al. 2009). Also, regular seasonal and inter-annual sampling would permit dust event impacts upon the upper atmosphere to be examined throughout the Martian year, and over several Mars years. This would enable a climatology of upper atmosphere structure and its variations via coupling with the lower atmosphere to be assembled, in much the same way as is already underway for the Mars lower atmosphere (e.g. Liu et al. 2003; Smith 2004, 2009; Smith et al. 2014).

Sections 3.1.1 (NGIMS) and 3.2.1 (IUVS) contain a discussion of MAVEN measurements that will be made to constrain these wave features in the upper atmosphere structure. In addition, the MAVEN Accelerometer Experiment (ACC) will be used to derive mass density variations that can be used to constrain these same wave features (see Zurek et al. 2014, this issue).

2.1.4 What Is the Global Thermospheric Neutral Wind Structure and How Does It Vary Both Spatially and Temporally?

Neutral thermosphere winds are also important to measure systematically over all local times and latitudes, over a regular sampling of Mars seasons, and throughout the solar cycle. How-

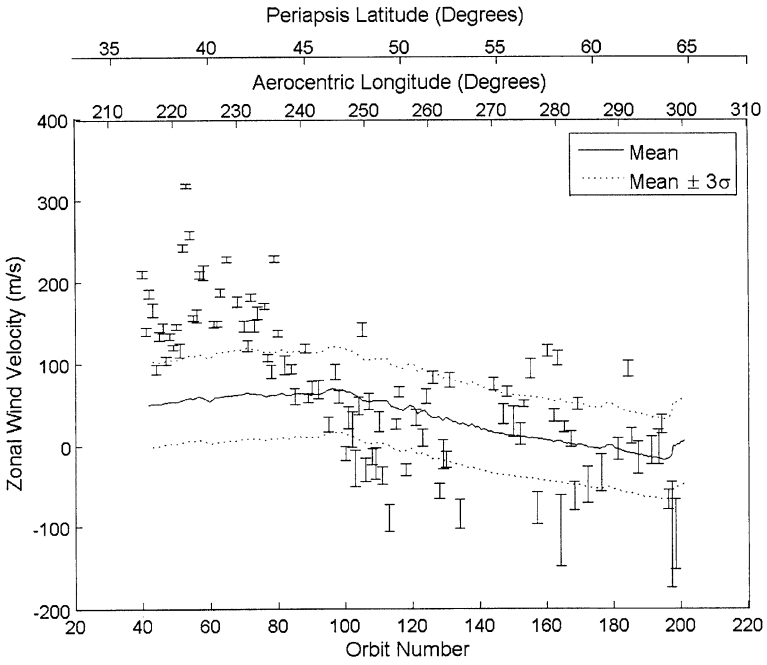

Fig. 6 Zonal winds derived from MGS IMU and gyro rate datasets acquired during the same Noachis dust storm event illustrated in Fig. 5. Zonal winds (*with error bars*) are plotted and compared to MARSGRAM computed mean zonal winds (*solid curve*) and 3-σ variations (*dotted curves*) about the zonal wind mean value. *Taken from Baird et al.* (2007)*, Fig. 9. Journal of Spacecraft and Rockets*

ever, thermospheric (in-situ) neutral wind measurements are presently lacking. When such winds are available to be combined with simultaneous neutral density and temperature measurements, they enable 3-D models to identify/quantify the intricate feedbacks of energetic, chemical, and dynamical processes in the upper atmosphere (Bougher et al. 2008, 2014). Wind measurements are also necessary to establish the baseline to identify changes that may occur in response to special events driven by dust storms and solar activity. In fact, studies utilizing MGS IMU plus gyro rate datasets were used to unfold zonal wind speeds during the Noachis dust storm event (1997–1998); i.e. these zonal winds (see Fig. 6) doubled from ∼100 to 200 m/s during the onset of the storm and relaxed back toward pre-storm levels over the following ∼6–8 weeks (e.g. Baird et al. 2007; Zurek et al. 2014, this issue). Global horizontal wind patterns can also be inferred (estimated) based upon density, temperature, and airglow distributions (see Bertaux et al. 2005a, 2005b; Bougher et al. 2006, 2014). However, we presently lack the global measurements of detailed thermospheric parameters (i.e. temperatures, densities, winds) that provide comprehensive constraints for 3-D global models.

MAVEN will not make in-situ thermospheric wind measurements. However, the Accelerometer Experiment (ACC) will use IMU and spacecraft attitude control datasets to derive torques that can be used to estimate cross-track winds during the Deep-Dip campaigns (see discussion in Zurek et al. 2014, this issue).

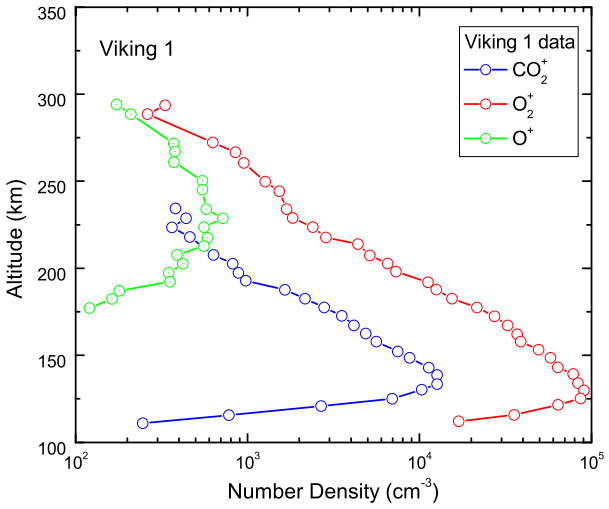

Fig. 7 Viking Lander 1 ion density profiles measured by the RPA instrument. *Adapted from Hanson et al.* (1977)*, Fig. 6a. J. Geophys. Res., American Geophysical Union*. O_2^+, CO_2^+, and O^+ are plotted as measured upon descent by the VL1 spacecraft

2.2 Ionosphere

2.2.1 What Is the SZA (Solar Zenith Angle) Dependence of the Ionospheric Densities and Altitude Profiles, as Well as Variations with the Mars Seasons and Solar Cycle?

Many basic ionospheric properties and processes are poorly constrained by existing observations (see reviews by Withers 2009; Haider et al. 2011; Bougher et al. 2014). The only existing in-situ data on the composition, temperatures and motions of the Martian ionosphere still consist of the two altitude measurement profiles (including densities of O_2^+, CO_2^+, and O^+) from about 110 to 300 km as measured by the Retarding Potential Analyzers (RPA) on the Viking 1 and 2 Landers near 44° SZA at low solar activity (see Fig. 7) (e.g., Hanson et al. 1977).

By contrast, many electron density profiles from the ionosphere of Mars have been obtained by radio occultation (RO) experiments (over a wide range of solar cycle conditions) beginning with the Mariner 4 flyby in 1964 and continuing to Mars Express (2004–present) (e.g., Fjeldbo and Eshleman 1968; Barth et al. 1992; Hinson et al. 1999; Pätzold et al. 2005; Mendillo et al. 2003, 2013). Also see reviews by Withers (2009), Haider et al. (2011), Bougher et al. (2014). The early measurements from Mariner 9 and Viking gave indications of solar cycle variations of the ionospheric profiles, and revealed a very weak (often not measurable) and variable nightside ionosphere (e.g. see Zhang et al. 1990a, 1990b and references therein). From 1998 to 2005, the Mars Global Surveyor (MGS) Radio Science Subsystem (RSS) returned ∼5600 high-latitude electron density profiles in the SZA range 71–89° (e.g., Hinson et al. 1999). Also, the radio science experiment MaRS on the European Mars Express (MEx) orbiter returned ∼500 electron density profiles during 5 Earth occultation seasons spanning the period from April 2004 to September 2008 (e.g., Pätzold et al. 2005).

MEx also employs the Mars Advanced Radar for Subsurface and Ionospheric Sounding (MARSIS) instrument to measure the topside ionospheric electron density profile and the peak density by vertical sounding (e.g. Gurnett et al. 2008). An advantage of the MARSIS experiment is that it can access regions of the ionosphere that RO experiments cannot for geometrical reasons: the deep nightside ionosphere (SZA > 125°) and the region near the

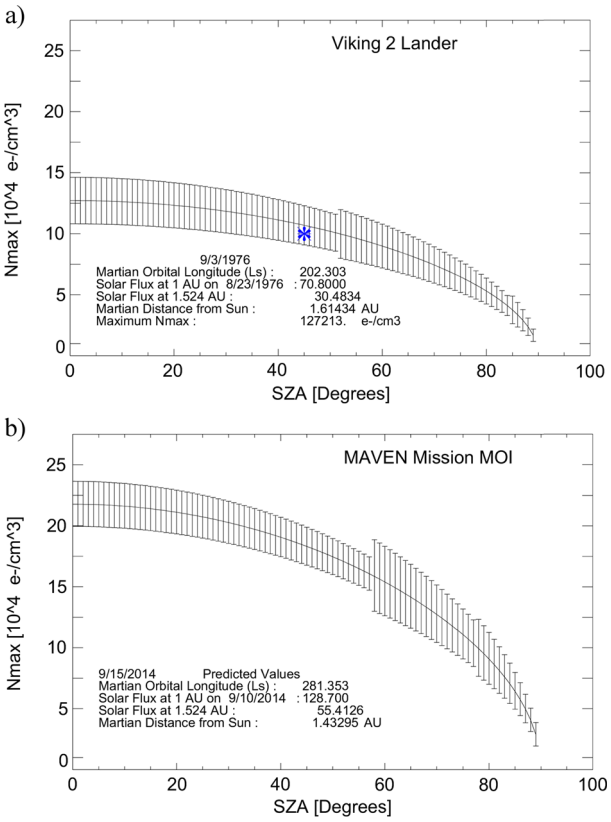

Fig. 8 Examples of Mars International Reference Ionosphere (MIRI) outputs for peak electron densities (N_{max}) as a function of SZA for a specific input conditions corresponding to: (**a**) the Viking 2 lander, and (**b**) the MAVEN arrival at Mars. Both input and outputs parameters are shown, and the *blue asterisk* gives the N_{max} values at the SZA of the Viking 2 lander. The uncertainty levels come from parameterizations of observed variabilities and for predictions of solar cycle F10.7 uncertainties. *Taken from Mendillo et al.* (2013)*, Fig. 2. Geophys. Res., Lett., American Geophysical Union*

subsolar point (SZA $< 45°$). MARSIS has enabled improved studies of the SZA behavior of electron density peak magnitudes and heights to be conducted (e.g. Morgan et al. 2008). In addition, in-situ electron densities can be extracted from MARSIS using a plasma wave technique (Duru et al. 2008).

Most recently, Mendillo et al. (2013) have initiated an effort to use MARSIS/AIS-mode observations (spanning a range of solar zenith angles, solar fluxes, and seasons) to begin the formulation of a Mars International Reference Ionosphere (MIRI) model. Nearly 113,000 values of maximum electron density (N_{max}) obtained from 2005 to 2012 are presently utilized. Validation studies using several radio occultation measurements (e.g. MGS) and Viking in-situ observations provide initial confirmation of a useful MIRI climatological model. This semi-empirical model can be applied to extract the major trends and characterize the variability of the ionospheric structure for both past observations and predictive cases (see Fig. 8). However, systematic global coverage is still lacking as is knowledge of the physical parameters (ion composition, temperatures, atmospheric composition) needed for definitively understanding the underlying physics.

A full characterization of Martian electron and ion density profiles (from ~100–400 km) is needed that requires spacecraft measurements that systematically span a range of local times and latitudes (effectively SZA), a regular sampling of Mars seasons, and range over a significant portion of the solar cycle. Such measurements would expand the identification of ion species in the Mars upper atmosphere and describe (quantify) their behavior. In par-

ticular, hydrogen (H_2) induced changes to ion composition are important (e.g. Matta et al. 2013) and should be characterized for the Mars. This expanded coverage would also provide a confirmation of the SZA dependence (e.g. Morgan et al. 2008; Mendillo et al. 2013) of basic features of the ionosphere (e.g. electron and ion species distributions, peak heights and magnitudes, ion layers), and investigate the temporal variability of these electron/ion densities and including their day-night distributions. In addition, the MIRI model can be updated and expanded to include MAVEN electron density datasets. Although MAVEN's baseline orbit will not penetrate to 100 km, UV limb scans may be able to provide useful compositional measurements below the ionosphere peak and MAVEN's detailed measurements of ionospheric/atmospheric parameters and solar inputs at periapsis will allow more accurate modeling of the lower altitude ionosphere regime. Sections 3.1.1 (NGIMS), 3.1.2 (LPW) and 3.1.3 (STATIC) contain a discussion of MAVEN measurements that will be made to provide an expanded characterization of Martian electron and ion density structure and variability.

2.2.2 *What Are the Global Distributions of Thermal Ion and Electron Temperatures and How Do They Vary Both Spatially and Temporally?*

Measurements of Mars electron and ion temperatures are also limited to two profiles returned from the RPAs on the Viking 1 and 2 landers (e.g. Hanson and Mantas 1988) (see Sect. 2.2.1). Some form of these plasma temperature profiles are still used today in most ionospheric model calculations, regardless of the SZA location or solar cycle conditions. Electron temperature datasets (including temporal and spatial variations) are very important to obtain, since they have a strong impact on dissociative recombination (DR) rates, as a function of altitude, for molecular ion species (e.g. O_2^+, CO_2^+, N_2^+, CO^+, NO^+). It is noteworthy that DR of O_2^+ is the primary source of hot O atoms at Mars, which is included in exosphere models for calculating escape fluxes and global escape rates (e.g. Nagy and Cravens 1988; Fox and Hać 2009, 2010; Valeille et al. 2009a, 2009b, 2010a, 2010b; Yagi et al. 2012). In addition, electron and ion temperatures are needed to determine the thermal plasma pressure in the ionosphere, which is a key forcing term in the plasma dynamics and plays an important role in the solar wind interaction with Mars.

A global characterization of these plasma temperatures is needed in combination with the density measurements described above. Sections 3.1.2 (LPW) and 3.1.3 (STATIC) contain a discussion of MAVEN measurements that will be made to provide an expanded characterization of Martian electron and ion temperatures (respectively) and their variability.

2.2.3 *What Are the Global Ionospheric Flows and Their Variations with Solar Cycle and Mars Seasons?*

Reliable data on Mars plasma motions is entirely absent except for some very sparse deductions from the Viking RPA's (e.g. Hanson et al. 1977). Trans-terminator ion flow is likely to exist on Mars (e.g. Fränz et al. 2010), but maybe not to the same degree at all terminators as Venus, owing to the Mars crustal magnetic fields and the absence of planetary rotation on Venus. Ion flow datasets were found to be crucial at Venus for understanding the mechanisms responsible for maintaining the nightside ionosphere (see review of Fox and Kliore 1997). Mars ion flow may contribute to the near terminator (and maybe deeper nightside) ionosphere structure as well (e.g. Němec et al. 2010, 2011). Information on the cross-terminator flows is essential to distinguishing the transport source of ionization from the suggested particle precipitation sources of the nightside (e.g., Fox et al. 1993; Dobe et al. 1995; Fox 2009;

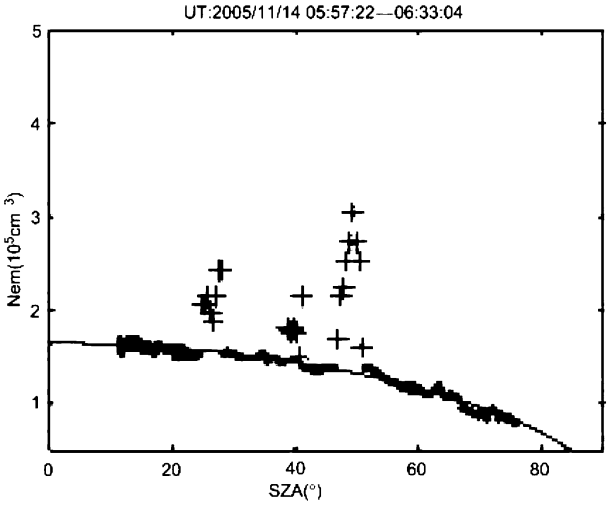

Fig. 9 Peak electron densities, N_m, measured by the MARSIS AIS mode as a function of SZA (χ) over roughly 36 minutes on 14 November 2005. *Dots* indicate values of peak electron density (N_m) that are close to their expected values; *crosses* indicate values of N_m that are significantly larger than their expected values. The *solid line* shows a fit of the data points to a function of the form $N_m = N_0 \cos(\chi)^{0.5}$. *Taken from Nielsen et al.* (2007)*, Fig. 1. Planetary and Space Science*

Ma and Nagy 2007; Fränz et al. 2010; Haider et al. 2011). Moreover, it must be determined whether these flows are a result of ionospheric thermal pressure gradients (as for Venus at solar maximum conditions), or are controlled mainly by the solar wind interaction through penetrating magnetic and electric fields. It is also important to evaluate the ion (neutral) drag forces that will feed back into the neutral (ion) dynamics. Currently the global models of the thermosphere, even those containing the ionosphere, do not include drag feedback effects that must become significant at some altitudes.

Measurements of the ionospheric flows, covering as much of the terminator region as possible, and including latitude and solar cycle coverage, are necessary to establish the extent to which the dayside is the source of the nightside ionosphere. These measurements must include supporting information, such as solar wind pressure and solar EUV fluxes, that will allow determination of the circumstances that control it from the outside. But they must also include information about the prevailing magnetization state of the ionosphere. Key MAVEN measurements addressing thermal ion flows will be obtained from STATIC (see Sect. 3.1.3).

2.2.4 How Is Ionospheric Structure Affected by the Crustal Fields?

Dayside ionospheric structures from MGS radio occultation measurements (∼130–200 km) reveal several "anomalous" profiles corresponding to abrupt changes in topside electron density with altitude above strong crustal magnetic fields (see Withers et al. 2005). Alternatively, Fig. 9 shows MARSIS peak electron densities, measured in the AIS mode, that are nearly twice as large as expected (see Nielsen et al. 2007). These enhancements are also associated with strong and vertical crustal fields, and are attributed to increased electron temperatures (yielding reduced dissociative recombination rates) at this location. Withers et al. (2005) conclude that the presence of strong magnetic fields is a necessary condition for the production of the anomalous MGS profiles. However, it is unknown whether the occurrence of such anomalous features in some, but not all, profiles above strong crustal fields is due to some combination of solar wind conditions and crustal field magnitudes, or some other physical process.

As discussed above, the sources of the nightside ionosphere are assumed to be similar to those at Venus: transport of ions from the dayside or precipitation of energetic particles

(see reviews by Withers 2009; Haider et al. 2011; Bougher et al. 2014). However, energetic particle precipitation at Mars is subject to the crustal magnetic field topology. Fillingim et al. (2007) proposed that nightside ionization would be localized and patchy, due to precipitation of solar wind electrons mainly in regions of open (nearly radial) magnetic field lines, and the absence of ionization in regions of closed (or horizontal) magnetic fields. Safaeinili et al. (2007) came to a similar conclusion, when they analyzed MEX MARSIS data to determine the total electron content (TEC) of the nightside ionosphere. This patchiness may partially explain the existing orbits for which RO measurements did not detect a well defined nightside ion density peak (e.g. Němec et al. 2010). In addition, MHD models of the global solar wind interaction including the ionosphere (see Ma et al. 2004; Ma and Nagy 2007; Najib et al. 2011; Dong et al. 2014) suggest that the ionospheric flows on the dayside will be affected by the stronger crustal fields' presence. These effects may range from simple flow deflections to turbulence in regions of stagnation, flow convergence, or shear.

Systematic thermal ion/electron density measurements, along with supra-thermal electron spectra, are needed (with high temporal and spatial resolution) to confirm and characterize the nightside ionosphere patchiness and its relation to particle precipitation in regions of nearly radial magnetic fields, and to investigate the more global ionospheric flow influences of the Martian crustal magnetization. Sections 3.1.1 (NGIMS), 3.1.2 (LPW) and 3.1.3 (STATIC) contain a discussion of MAVEN measurements that will be made to provide an expanded characterization of Martian thermal electron and ion densities and their variability. Suprathermal electron measurements will be obtained by SWEA (see Mitchell et al. 2014, this issue). Magnetic field measurements will be made by MAG (see Connerney et al. 2014, this issue).

2.2.5 *How Does the Upper Boundary of the Ionosphere, the Ionopause, Vary Spatially and Temporally?*

The transition between the main ionosphere and the shocked solar wind is complex and not fully-understood. Nonetheless, this boundary has been defined in a couple of ways (see review by Brain et al. 2014). The first relies on the fact that ionization of atmospheric CO_2 and O produces electrons with specific energies (Mitchell et al. 2000). The presence of these photoelectrons (along with tracing along magnetic field lines) is used as a tracer of the ionosphere, and the transition between regions where photoelectrons are evident and where they are lacking is termed the photoelectron boundary (PEB). The PEB ranges in altitude from ∼150 to 1500 km, but has a median value of ∼380 km (Mitchell et al. 2001). In short, the PEB can be considered a boundary separating flux tubes containing significant quantities of solar wind electrons from those containing only ionospheric photoelectrons (Brain et al. 2014).

Alternatively, and similar to Venus, an ionopause can be defined where the ionospheric electron density decreases rapidly with height (see review by Brain et al. 2014). Steep gradients in local electron density, similar to those observed at Venus, are sometimes (but not usually) evident in MEx MARSIS observations. Instead, a transient and spread-out transition, or "ionopause" (Duru et al. 2009) is more often present. Furthermore, MARSIS in-situ observations can provide an additional (limited) view of the upper edges of the ionosphere and its variations (Duru et al. 2009, 2010). Nevertheless, they indicate the Mars topside ionosphere is not generally characterized by a sharp ionopause gradient in density, clearly different than Venus during solar maximum conditions. Thus far, the average measured Mars ionopause altitude is almost constant on the dayside (∼450 km), and increases near the terminator. Also, the ionopause height is observed to rise in regions where strong crustal fields are located (Brain et al. 2014).

The transient nature of this boundary, and the underlying processes that control the altitude variation, are not well understood in part because of the large number of controlling parameters (see Brain et al. 2014). For example, exploration of the influence of the Martian crustal fields and their variable plasma interaction geometry, with an independently variable interplanetary field orientation, has so far only been accessible through modeling. Details such as plasma velocity shear and density gradient size may also be a factor outside of crustal regions if the Kelvin Helmholz instability occurs near the Martian ionopause flanks as it is proposed to occur at Venus (e.g. Penz et al. 2005).

A wide variety of MAVEN measurements are planned that systematically (a) sample the photoelectron spectrum (SWEA), and (b) the electron density variations throughout the dayside and nightside upper ionosphere regions (LPW), taking the local and global crustal magnetic field context into consideration. Corresponding electron temperature (LPW), magnetic field (MAG), ion composition (NGIMS, STATIC) and ionospheric flow measurements (STATIC) are slated to help diagnose cause and effect in producing the observed ionospheric boundary characteristics. Even then, statistical results with wide coverage are needed to establish global context. These measurements will also span the Mars seasons and range over a wide variation in solar radiation fluxes in order to capture changing solar cycle impacts upon the ionospheric thermal pressure. Finally, monitoring of upstream solar wind conditions is planned (SWEA, SWIA, SEP, MAG) to constrain the changing behavior of the solar wind dynamic pressure and interplanetary magnetic field (see Mitchell et al. 2014; Halekas et al. 2013, this issue; Larson et al. 2014; and Connerney et al. 2014). MAVEN thermal ion and electron measurements (densities and temperatures) are discussed in Sects. 3.1.1 (NGIMS), 3.1.2 (LPW), and 3.1.3 (STATIC).

2.2.6 How Does the Thermosphere-Ionosphere Respond to Episodic Solar Events (e.g. Solar Flares, CMEs, etc.)?

The response of Earth's upper atmosphere to solar activity-related events, specifically flares and coronal mass ejections (CMEs) is well documented (see review by Fuller-Rowell and Solomon 2010). Flare response is fairly straightforward because it is mainly a response to impulsive solar EUV and X-ray flux enhancements. It is seen most easily in radio occultation electron density profiles. For example, Martian MGS radio occultation electron density profiles were acquired within minutes of a solar flare on 15 April 2001 (X14.4 class flare) and 26 April 2001 (M7.8 class flare) (Mendillo et al. 2006). See Fig. 10. At Mars, the primary electron density layer, produced by EUV ionization, typically shows a peak near ~120–135 km (local noon) and is sometimes referred to as the F_1 layer (or M_2 layer), after an Earth-based (Mars-based) nomenclature (e.g. Bougher et al. 2014). Likewise, a secondary layer, sometimes visible with a peak near ~110 km, and produced by highly variable X-ray ionization and associated electron impact ionization, is known as the E layer (or M_1 layer) (see Pätzold et al. 2005). From the passage of these solar flares, the electron densities above the F_1 layer did not change by more than the measurement uncertainties, yet the electron densities in the E-layer region were significantly increased (doubled at 100 km) (Mendillo et al. 2006). This enhancement was relatively short-lived (minutes to hours). The neutral atmosphere effects of this ionization enhancement are likely modest to insignificant, but haven't been investigated by measurements. Predictions of Martian atmospheric impacts (both neutral and plasma) resulting from solar flare events are beginning to be made using 3-D thermosphere-ionosphere model simulations (e.g. Pawlowski and Bougher 2012; Ma et al. 2014).

In the case of CMEs, the Earth's relatively strong global dipole field plays a major role in organizing the system's response and all of its forms; i.e. this includes the polar auroral oval,

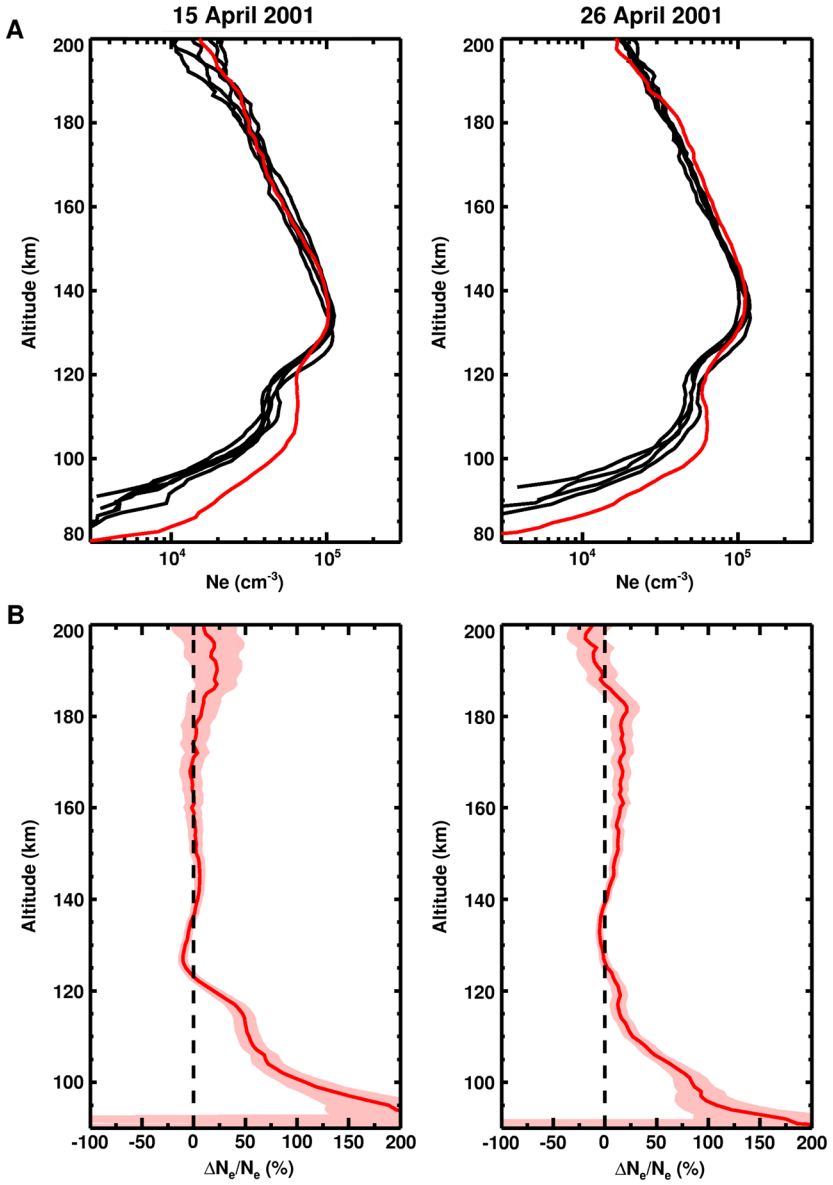

Fig. 10 (**a**) MGS radio occultation electron density profiles acquired within minutes of a solar flare on 15 April 2001 (X14.4 class flare) and 26 April 2001 (M7.8 class flare). Measurement uncertainty is several 1000 electrons per cm^3, and thus the two profiles in *red* (14:15 and 13:16 UTC, respectively) show statistically significant departures at low altitudes because of solar flares; (**b**) Percentage differences between flare affected profiles and the averages of the other profiles on each day. The shadings give the 1-σ standard error in the relative change in electron density. *Taken from Mendillo et al.* (2006)*, Fig. 1. Science*

atmospheric energy deposition, induced ionospheric and magnetospheric currents, and radiation belt energizations that produce thermospheric responses (see review by Fuller-Rowell and Solomon 2010). However, the weakly magnetized planets have their own distinctive re-

sponses that are still only partly understood. For example, at both Venus and Mars, there is deeper penetration of the interplanetary magnetic field (IMF) into the upper atmosphere as well as reduction of the ionopause boundary altitude during the passage of a CME disturbance owing to its high solar wind dynamic pressure and enhanced fields (e.g. Crider et al. 2004). The responses of the Venus ionosphere to such magnetization, which can last for hours to days, includes an apparent reduction in the cross-terminator transport of dayside ionospheric plasma into the nightside ionosphere. However the consequences for the Mars nightside ionosphere and resultant thermospheric responses are not known.

Instead, there are only model-based predictions for potentially large effects of such 'space weather' impacts on both the Mars upper atmosphere properties (e.g. Fang et al. 2013) and related atmosphere escape (e.g. Ma and Nagy 2007; Wang et al. 2012; Fang et al. 2013; Lillis et al. 2014). A major energy input, unique to the weakly magnetized planets, is from precipitating pickup ions that impact the atmosphere instead of escaping into the solar wind (see Fang et al. 2013 and Lillis et al. 2014, this issue).

Finally, solar active region (i.e. 27-day solar rotation) effects are also important for the Mars ionosphere structure and its variability. Evidence of these effects is provided in recent work by Mendillo et al. (2013) and others.

In short, high temporal "campaign style" sampling of the Martian upper atmosphere structure is needed to capture the responses to episodic solar events, together with information about the solar flares and CMEs affecting Mars orbital location. Coordinated neutral and ion measurements (around the globe) are needed to investigate the time-variable responses on the both the dayside and nightside and how they propagate around the planet. These episodic events are also extremely important to systematically measure and study, because they may be key to the MAVEN goal of understanding how escape to space has affected the long-term evolution of the Martian atmosphere (if their effects significantly alter the escape rates). They also provide an excellent method to test our ideas about response times and heating/cooling mechanisms that control the upper atmosphere structure, energetics and dynamics (e.g. Pawlowski and Bougher 2012; Ma et al. 2014).

2.2.7 How Does the Thermosphere-Ionosphere Respond to Dust Storm Events?

The dayside thermosphere was sampled using the MGS accelerometers during the onset and decay phase of the Noachis regional dust storm in 1997–1998 (e.g. Keating et al. 1998; Bougher et al. 1999a) (see Sect. 2.1.4). Measured mass densities at a constant altitude (130 km) were enhanced by factor of ∼3 in a few days, and decayed gradually over the following few weeks toward pre-storm values (see Fig. 5). This "blooming" effect of the neutral thermosphere during dust events is accompanied by a corresponding impact on the embedded ionosphere. The electron density (F_1) peak altitudes are observed to rise during regional or global dust storms in the lower atmosphere as seen during the Mariner 9 primary mission and the early part of the Viking mission (Kliore et al. 1972; Zhang et al. 1990a). For the Mariner 9 primary mission, F_1 peak heights were reported in the range from ∼134 to ∼154 km for a SZA of 50° to 60° (Kliore et al. 1972), which is ∼20–30 km higher than average. Also, during the onset of the 1997–1998 Noachis regional storm, the MGS accelerometer found the height of the dayside 1.26-nbar level was raised by ∼10 km (Keating et al. 1998). This is consistent with an ionospheric peak altitude that is also raised by this same amount. Most recently, MGS radio occultation sampling during a regional dust storm event (during MY27, around Ls = 230) revealed an initial rise of the dayside F1-peak altitude by about ∼5 km. See Fig. 11. Further characterization of such dust storm impacts upon the Mars ionosphere will require high temporal "campaign style"

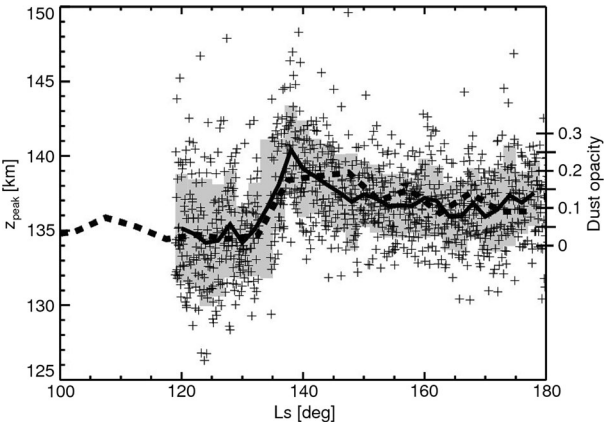

Fig. 11 Ionospheric peak altitudes measured at latitudes 62.4°N to 80.1°N by the MGS radio occultation instrument during the dust storm that perturbed SPICAM density and pressure measurements at Ls = 130° in MY 27. Data are shown as *crosses*. Mean altitudes for 2° wide Ls bins are shown by the *thick solid line*. The standard deviation in the peak altitude for each of these bins is shown by *shaded gray boxes*. The *dashed line* shows the average tropical dust opacity from Fig. 5 of Withers and Pratt (2013). *Taken from Withers and Pratt* (2013)*, Fig. 9. Icarus*

sampling of the thermosphere-ionospheric structure in order to capture the time-variable responses during storm onset and decay.

A wide variety of MAVEN measurements (thermosphere-ionosphere-exosphere, and solar wind interaction region) will be studied together to understand the whole atmosphere response to episodic dust storm events. Such events are extremely important to systematically measure and understand. As was stated above, they provide excellent (time variable) constraints against which to test ideas about the intricate feedback of global neutral-ion composition, temperature, and wind fields that control the upper atmosphere structure (e.g. Bougher et al. 2011a, 2011b; Pawlowski et al. 2011; Pawlowski and Bougher 2012). They also are a potentially important part of understanding how and why atmospheric escape is influenced by these events.

2.3 Exosphere

2.3.1 What Are the Global Distributions of Hot (Suprathermal) Neutral Species (e.g. Hot O, N, C, H)? How Do These Distributions Vary with Solar Cycle, Season, and Shorter Timescales Including Episodic Events?

Pioneer Venus Orbiter UVS datasets were used to constrain the hot atomic coronae (O, C, H) of Venus (e.g. Nagy et al. 1981; Bertaux et al. 1985; Paxton 1985). On the other hand, owing to a lack of data, the hot atom coronae of Mars have only been modeled using Venus as an analogy (e.g. Nagy and Cravens 1988). Both 1-D and 3-D exosphere models, with widely varying complexity, have recently been used to simulate the hot atomic O distribution as well as the corresponding escape fluxes and global escape rates (e.g. Kim et al. 2001; Hodges 2002; Krestyanikova and Shematovitch 2005; Cipriani et al. 2007; Chaufray et al. 2007; Valeille et al. 2009a, 2009b, 2010a, 2010b; Yagi et al. 2012). Fox and Hać (2009) also compute hot O escape fluxes and global escape rates. Even today, the amount of data available characterizing Mars' extended upper atmosphere (exosphere) is very limited. For in-

stance, an exospheric atomic O profile was derived recently from measurements of 130.4-nm emission observed by Feldman et al. (2011) with Rosetta-ALICE.

The hot atomic coronae (e.g. O, N, C, H) in the exosphere of Mars are important for understanding the overall interaction of the solar wind with Mars, the structure of the extended upper atmosphere, volatile escape rates from the atmosphere and their relation to its long-term evolution. In addition, models suggest that episodic solar events will lead to exospheric enhancements from processes such as sputtering (Wang et al. 2012) or upper atmosphere heating or ionization by increased pickup ion precipitation (Fang et al. 2013). Dust storms may also have an impact, as they do on the thermosphere-ionosphere.

What is needed is a systematic sampling of global exospheric atomic (e.g. O, N, C, H) density (both cold and hot) distributions (i.e. across both dayside and nightside), over a variety of Mars seasons, and throughout the solar cycle. Both in-situ (lower altitude) and remote (higher altitude) measurements are required to characterize their behavior. Only then will the spatial and temporal coverage necessary to characterize the changing exospheric density distributions, and to subsequently estimate hot atom escape rates making use of modern exospheric models, be in hand (see reviews of Bougher et al. 2008; Brain et al. 2014). Section 3.2.1 describes IUVS measurements that will be obtained to constrain these hot atom (coronal) distributions.

3 What Specific Measurements by MAVEN Instruments Will Address These Open Questions?

The MAVEN mission is slated to obtain in-situ measurements of the composition, densities, and scale heights of the major neutral and ion species (NGIMS, STATIC), ion temperatures and velocities (STATIC), as well as electron densities and temperatures (LPW). Each of these in-situ measurements will be made along the orbit track, whose periapsis migrates around the planet during the course of the primary mission (see Fig. 1 from Zurek et al. 2014, this issue), providing a systematic spatial coverage over most latitudes and local times. The elliptical orbit with an apoapsis above ~6000 km, nominal periapsis near ~150 km, and 5-campaigns with periods of "deep dipping" down to ~120 km, allows direct in-situ sampling of the entire reservoir region. These "deep dipping" campaigns are designed to provide sampling at/below the homopause and are dispersed throughout the MAVEN primary mission: subsolar region, dawn/dusk terminators, anti-solar region and the South pole (see Zurek et al. 2014, this issue). Finally, this in-situ sampling will be conducted during changing solar fluxes during the declining phase of solar cycle #24, and throughout the seasons covering half the Martian year (Ls ~ 230 to 60°). See Sect. 3.1.

These "point" measurements will be extended to a global scale using remote-sensing (IUVS) measurements of the entire visible disk (see Sect. 3.2). Retrieval techniques making use of prominent Martian dayglow emissions have also been utilized as an efficient tool to extract neutral O and CO_2 densities (see Sect. 2.1.2). These same techniques will also be exploited (and expanded to other density retrievals) making use of IUVS limb profiles (see Sect. 3.2).

3.1 In-situ Measurements

3.1.1 NGIMS (Only Below ~500 km)

The details of the NGIMS (Neutral Gas and Ion Mass Spectrometer) instrument heritage, design, performance, and operations, are outlined elsewhere (see Jakosky et al. 2014 and

Mahaffy et al. 2014, this issue). Here we outline the relevant parameters measured, and their importance for characterizing the reservoir available for escape.

The NGIMS instrument will measure the neutral composition of the major gas species, and the thermal ions in the Martian upper atmosphere. This includes density profiles of He, N, O, CO, N_2, O, O_2, Ar and CO_2, and their major isotopes from the homopause up to about one scale height above the "traditional" exobase, with a vertical resolution of ~5 km and a target accuracy of ~25 % for most of these species (Mahaffy et al. 2014, this issue). Neutral temperatures (Tn) will be derived from neutral scale heights. Likewise, NGIMS will measure density profiles of thermal O_2^+, CO_2^+, NO^+, O^+, CO^+, C^+, N_2^+, OH^+, and N^+ from the primary (F1) peak near ~120 km up to the average ionopause height (~400–500 km) (see Sect. 2.2.5) with a vertical resolution of ~5.0 km (Mahaffy et al. 2014, this issue). Measurements of targeted species will typically be secured at a cadence of at least 2 measurements (but typically many more) for each scale height below ~400–450 km, with unit mass resolution and with negligible crosstalk from an adjacent unit mass signal. The NGIMS has the capability to measure any m/z values from 2 to 150 Da although typically the mass range between 2 and 60 Da will be most intensively sampled. On selected orbits, NGIMS measurements will cycle regularly between neutrals and ions while on other orbits only neutral gases will be measured. The cadence of this cycling will be tested, but likely will oscillate between orbits with sampling using: (a) Closed Source (CS) neutrals plus Open Source (OS) neutrals, and (b) OS (ions) plus CS (neutrals). Sequence (a) will enable the response of the open source to be normalized against that of the closed source for inert gases and correct for any sensitivity changes in the open source due to neutral winds. The sensitivity of each NGIMS ion source is $2–3 \times 10^{-2}$ (counts/second)/(particle/cc) for a gas that ionizes with the efficiency of argon. Background spectra will be secured before and after atmospheric entry on each orbit.

These NGIMS in-situ measurements, with the spatial and temporal coverage outlined above, will systematically characterize the features and the time variable behavior of the reservoir region (i.e. thermosphere-ionosphere). Specifically, NGIMS will determine the variation of the neutral composition with altitude, latitude, local time, longitude and season from the homopause upward into the exosphere where neutral escape can occur (see Sect. 2.1.2). Variations across a range of solar cycle conditions will also be monitored. These measurements will subsequently provide valuable constraints for numerical model studies of thermospheric energetics, transport, global circulation, and the formation of the dayside and nightside ionosphere. From these studies, the processes responsible for driving upper atmosphere responses to both periodic and transient solar forcing mechanisms can be investigated (see Sects. 2.1.1, 2.1.2, 2.2.1, 2.2.6). In addition, these in-situ upper atmosphere measurements will reveal the impacts of upward propagating tidal and planetary waves, as well the passage of dust storm events, from the lower atmosphere. Such impacts are thought to significantly modify the structure and dynamics of the upper atmosphere, beyond that driven solely by solar forcing (see Sects. 2.1.3, 2.1.4 and 2.2.7). In short, the systematic characterization of the reservoir region, provided in part by the NGIMS instrument, is crucial to move forward with detailed studies of atmospheric loss processes and the determination of volatile escape rates (see Sect. 1.2).

3.1.2 LPW (SEUV Described Later in Sect. 3.3.1)

The details of the LPW (Langmuir Probe and Waves) instrument heritage, design, performance, and operations, are outlined elsewhere (see Jakosky et al. 2014 and Ergun et al. 2014). Here we outline the in-situ parameters measured, and their importance for characterizing the reservoir available for escape.

The LPW instrument will measure the thermal electron density (from a few hundred up to $\sim 3 \times 10^5$ cm^{-3}) and temperatures (from 300 K up to ~5000 K) from near the ionosphere primary (F_1) peak to the average ionopause altitude (~400–500 km) with a vertical resolution of one O_2^+ scaled height and 5 % accuracy (Jakosky 2008). In addition (not in-situ), electric field wave power will be measured at frequencies important for ion heating (~0.5 Hz to 500 Hz) with a sensitivity of 10^{-10} (V/m^2) below 500 Hz.

These LPW in-situ measurements, with the spatial and temporal coverage outlined above, will systematically characterize the features and the time variable behavior of the reservoir region (i.e. electron densities and temperatures). This is important for monitoring the changing nature of the ionopause location and the overall 3-D ionosphere structure (see Sects. 2.2.1, 2.2.5). Furthermore, electron temperatures are crucially important to the calculation of dissociative recombination (DR) rates (e.g. O_2^+ DR), from which hot atoms are produced and potentially escape from the exosphere (see Sect. 2.2.2). Model calculations of hot atom escape rates will be vastly improved with the advent of such a MAVEN database of global electron temperatures (see Sect. 2.3.1).

3.1.3 STATIC

The details of the STATIC (Supra-thermal and Thermal Ion Composition) instrument heritage, design, performance, and operations, are outlined elsewhere (see Jakosky et al. 2014 and McFadden et al. 2014). Here we outline the in-situ parameters measured, and their importance for characterizing the reservoir available for escape.

The STATIC instrument measures the velocity distributions and mass composition of both supra-thermal and thermal ions. When sampling below 500 km, density profiles of the major ions (H^+, O^+, O_2^+, CO_2^+), their corresponding ion temperatures (~0.02 eV to >10 eV), and the 3-component (X, Y, Z) ion flow velocities (~0.2 to 25 km/s) are measured (McFadden et al. 2014). For our purposes of characterizing the thermosphere-ionosphere reservoir, we are focused upon thermal ions that originate in the ionosphere (below the nominal ionopause). Here, measurements of thermal ions (O^+, O_2^+, CO_2^+) and ion flow velocities approaching the nominal ionopause will be important for characterizing the thermosphere-ionosphere reservoir. However, no other MAVEN instrument will provide ion temperatures that are crucial for calculating ion-neutral chemical reactions of the ionosphere.

3.2 Remote Measurements

3.2.1 IUVS

The details of the IUVS (Imaging Ultraviolet Spectrometer) instrument heritage, design, performance, and operations, are outlined elsewhere (see Jakosky et al. 2014 and McClintock et al. 2014). Here we outline the parameters measured, and their importance for characterizing the reservoir available for escape.

The IUVS is a remote sensing instrument that measures UV spectra (~110–340 nm) with four observing modes: (a) limb scans near periapsis, (b) disk mapping at high altitudes, (c) coronal scans, and (d) stellar occultations. The nominal spectral resolution is 0.6-nm in the FUV channel and 1.2-nm in the MUV channel, while the spatial resolution is ~4 km vertical on the limb and ~120 km horizontal at disk center from apoapsis (see McClintock et al. 2014). Products resulting from analysis of these spectra include column densities and vertical profiles of H, C, N, O, CO, N_2, and CO_2 (from the homopause up to a few

scale heights above the conventional exobase) and column densities and vertical profiles of C^+ and CO_2^+ (from within the ionosphere F1 layer). In addition, CO_2 scale heights can be used to derive temperatures from limb datasets. Accuracies of 0.5–3.0 % for density and 2–12 % for temperatures are achieved, depending on species. Stellar occultation measurements probe to lower altitudes, and provide CO_2, O_2, and O_3 density profiles. Temperatures are again derived from CO_2 scale heights and provide a means to monitor the variable thermal structure spanning the mesopause region (∼80–120 km) and a lower limit for the ion temperatures.

These IUVS measurements will provide a systematic mapping of the composition and structure of Mars neutral upper atmosphere and coronae (e.g. H, C, N, O). For the MAVEN primary mission, this mapping will span all local times and latitudes, sample about half of the Mars seasons (Ls ∼ 230 to 60°), and occur during the declining phase of solar cycle 24. Such a detailed spatial and temporal characterization of Mars' extended atmosphere, when combined with corresponding in-situ NGIMS and LPW thermosphere-ionosphere measurements, is precisely what is needed to properly constrain 3-D exospheric models from which photochemical escape rates can be calculated (see Sects. 2.1.1, 2.1.2, 2.2.1, 2.2.2, 2.3.1). The combined thermosphere-ionosphere-exosphere structure is crucial to characterize together, since spatial and temporal variations of the thermosphere-ionosphere strongly impact the resulting coronal distributions (and escape rates) of these light species (see Sect. 1.2). In addition, global neutral coronal distributions (e.g. hot O) are also crucial to measure in order to provide the source of pickup ions (O^+) for calculating ion escape using 3-D plasma models (see Sect. 1.2).

Lastly, the IUVS will measure the D/H ratio above the homopause with sufficient accuracy (∼30 %) to capture spatial and temporal variations (factor of 2) and compare with the measured D/H ratio in the bulk atmosphere (see Jakosky et al. 2014, this issue). Such measurements are crucial in order to constrain estimates of the loss of water from the atmosphere over Mars history.

3.3 Measurements Determining External Drivers

Specific MAVEN instruments will determine the external inputs that control the upper atmosphere and ionosphere structure, and that ultimately regulate atmospheric escape rates.

3.3.1 LPW/SEUV

The details of the LPW/SEUV (Solar Extreme Ultraviolet) instrument heritage, design, performance, and operations, are outlined elsewhere (see Jakosky et al. 2014 and Eparvier et al. 2014). Here we describe the solar irradiance measured, and its importance for characterizing the reservoir available for escape.

The LPW/SEUV instrument will measure solar irradiance at wavelengths important for ionization, dissociation, and heating of the upper atmosphere. Specifically, photodiodes at 3-spectral intervals will be used to measure solar irradiance at soft X-ray (0.1–7.0 nm), EUV (17–22 nm), and UV (Lyman-α) wavelengths with 10 % accuracy. The time resolution for sampling whenever pointed at the sun (1-s cadence) is sufficient to capture solar flares. These 3-channel measurements will be combined with the FISM model (e.g. Chamberlain et al. 2008) in order to reconstruct the entire solar spectrum from ∼0.1 to 195.0-nm (at least 1.0-nm intervals).

Solar flux measurements are crucial to obtain at Mars, in order to characterize the solar forcing that Mars upper atmosphere receives on any given sampling day from the side of

the sun facing the planet. When combined with thermosphere-ionosphere numerical models, these solar fluxes can be used as inputs for the calculation of ionization, dissociation, and heating rates. Subsequent comparison of model thermosphere-ionosphere outputs with other MAVEN datasets (i.e. NGIMS, LPW, STATIC) will enable heating/cooling processes and thermal structure to be much better constrained than at present (see Sect. 2.1.1). Furthermore, the variable solar flux impacts on the ionospheric structure can be measured, self-consistently modeled and the underlying physical processes examined in great detail (see Sect. 2.2.1). Finally, the time variable impacts of solar flares on both the thermosphere and ionosphere structure can be self-consistently investigated making use of NGIMS, LPW, and SEUV datasets in coordination with global thermosphere-ionosphere models (see Sect. 2.2.6).

Overall, the regular generation of complete solar spectra (0.1–195.0-nm) from these 3-photodiode proxy measurements (using the continually improving FISM model to fill in the gaps between the SEUV discrete measurements) will revolutionize our ability to model the structure of the Martian thermosphere-ionosphere system for comparison with specific MAVEN in-situ measurements. In addition, this coordination of MAVEN datasets and modeling will greatly enhance the global characterization of the reservoir that regulates volatile escape.

3.3.2 SEP

The details of the SEP (Solar Energetic Particle) instrument heritage, design, performance, and operations, are outlined elsewhere (see Jakosky et al. 2014 and Larson et al. 2014). Here we describe the solar particle energy spectrum measured, and its importance for characterizing the reservoir available for escape.

The SEP instrument measures the energy spectrum and angular distribution of solar energetic electrons (30–300 keV) plus protons and heavier ions (30 keV–6 MeV) presumably accelerated during solar flare and CME events. Fluxes of up to $\sim 3 \times 10^6$ cm^{-2} s^{-1} with an accuracy of $\sim$20 % are possible. A time resolution of 32-seconds is typical for monitoring, while an 8-s burst mode is available for SEP events in progress. With these measurements, this instrument will determine the SEP energy inputs (as a function of altitude) for quantifying episodic heating, ionization, and sputtering rates for the upper atmosphere. For instance, ions with energies up to 1 MeV are deposited above the homopause; ions with energies from 1–6 MeV are deposited below the homopause. Such rates are important to characterize and compare with solar flux (both periodic and transient) heating and ionization rates. Ultimately, these SEP episodic heating, ionization, and sputtering rates will be incorporated into thermosphere-ionosphere global models to examine the impact on upper atmosphere structure and dynamics. It is currently unknown what impact SEPs have on the upper atmosphere. However, the important SEP events accompany CMEs, and both may have been more frequent in the past when the Sun was likely more active. Thus the response to their presence will be examined together with the responses to the other solar events. Fortunately some SEP events arrive either in advance of or without the CME-associated solar wind disturbance, allowing one to investigate their separate effects on occasion.

4 Thermosphere-Ionosphere Sampling along MAVEN Orbit Trajectories

Thermosphere-ionosphere key parameters (KPs) are presently being simulated in coordination with the construction of the MAVEN model library for specific solar cycle, seasonal,

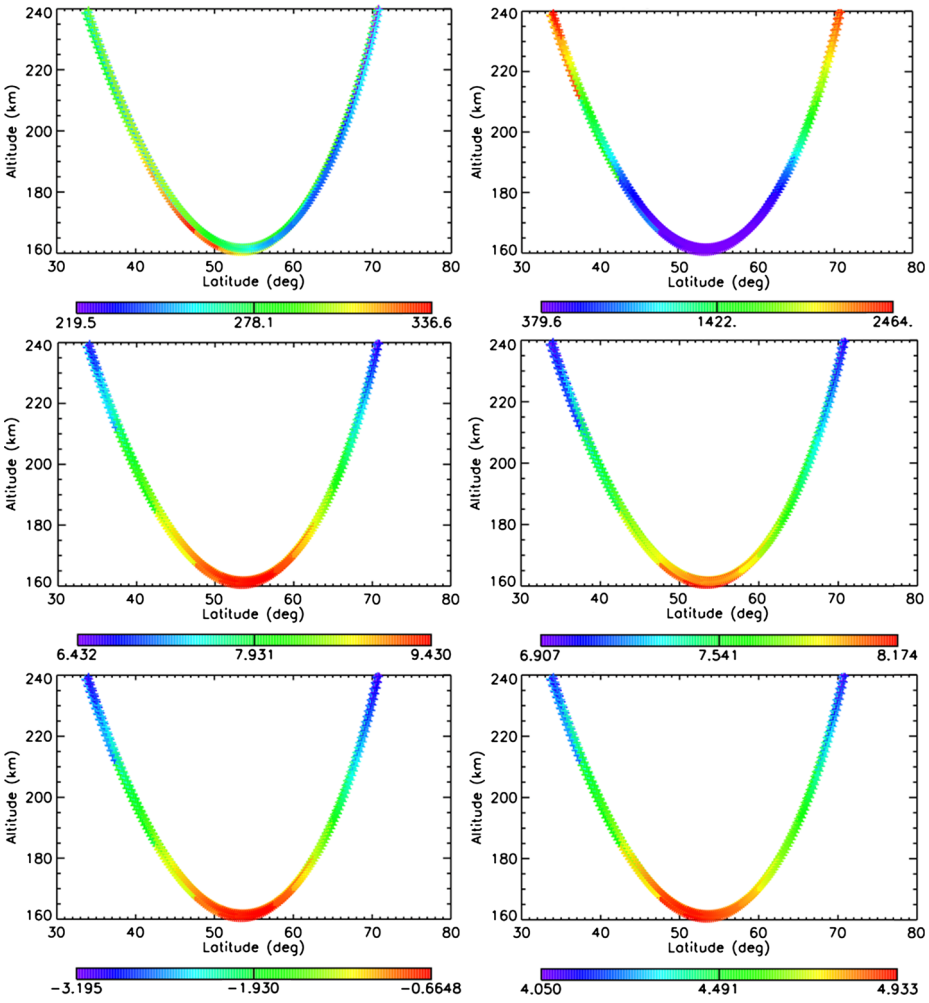

Fig. 12 MTGCM along the track (160–240 km) profiles of model key parameters (thermosphere-ionosphere) for the five MAVEN spacecraft orbit trajectories for Nov. 4, 2014: (**a**) neutral temperature (K), (**b**) electron temperature (K), (**c**) $\log_{10}$ CO_2 density (#/cm^3), (**d**) $\log_{10}$ atomic oxygen density (#/cm^3), (**e**) $\log_{10}$ mass density (kg/km^3), and (**f**) $\log_{10}$ electron density (#/cm^3). Six panel figure. The *color bars* indicate the magnitudes of the plotted model fields, including the minimum and maximum values

and dust conditions (see Lillis et al. 2014). Detailed comparisons of these parameters with corresponding in-situ measurements from the NGIMS, LPW, and STATIC instruments will eventually be conducted. Along the orbit track predictions of a few thermosphere-ionosphere KPs are presented here to illustrate the systematic method (and coverage) of sampling that will be achieved by the MAVEN in-situ measurements. Implications for subsequent data analysis strategies are briefly discussed.

Figure 12 illustrates outputs from the 3-D Mars Thermosphere General Circulation Model (MTGCM) thermosphere-ionosphere model (see Bougher et al. 2008; Bougher 2012)

for conditions generally appropriate to the first 2-months of MAVEN data taking operations (November–December 2014) spanning Ls $\sim 245 \pm 15°$. This period brackets the perihelion period of the Martian year, for which the solar declination is near its maximum southern extent. We assume solar moderate fluxes for this time period (F10.7 = 130 at Earth) and dust opacities corresponding to archived values from the MGS/Thermal Emission Spectrometer (TES) Year #1 measurements (Smith 2004). The latter selection imposes a horizontal distribution of integrated dust opacities outside of any dust storm event. Finally, a MAVEN spacecraft 4-sec trajectory file is utilized corresponding to all complete orbits (5) planned for November 4, 2014, early in the mission and soon after the start of MAVEN data taking. MTGCM fields are extracted and interpolated to the MAVEN trajectory points up to ~240 km (the approximate topside of the model domain).

The 6 panels illustrate the following parameters: neutral and electron temperatures (T_n, T_e), major neutral densities (O, CO_2), mass densities (ρ) and electron densities (N_e). Periapses for these orbits are near 53°N latitude, with an altitude of ~160 km, and a local time of ~10–11 AM. The inbound leg of each orbit is from the north. The included five orbits each sample about the same local time conditions for each inbound and outbound leg. However, the longitude migrates around the planet during the 5-orbits included. Thus, these orbit tracks (over 1-day) capture the combined altitude, latitude, and longitude variations of the parameters being measured.

From these 6-panels, we can extract a few key trends. Neutral temperatures are nearly isothermal above ~160 km, yet low latitude values are slightly warmer than those at higher latitudes. Horizontal variations are also visible along constant altitude levels on the outbound leg (~160–180 km). However, electron temperatures vary strongly with altitude above 160 km. Likewise, the O, CO_2, ρ and electron density tracks all reveal strong vertical variations that dominate any latitude and longitude variations that may be included. As the MAVEN orbit migrates in latitude and local time (see Fig. 1 from Zurek et al. 2014, this issue), one has the opportunity to combine data from several orbits (batches) and sort to extract variations separately as a function of latitude, local time, or longitude, etc. For example, constant altitude maps (latitude versus longitude) can be constructed from several orbits of data (batches) for which the local time range is narrowly confined. This removes the strong altitude and most local time variations in order to isolate latitude-longitude variations. Short term temporal variations are neglected (averaged out) in this exercise. This same strategy was used by the MGS, MO and MRO accelerometer teams to quantify latitude-longitude variations of mass densities that also varied strongly with altitude (e.g. Keating et al. 2008; Bougher et al. 2014).

In short, in-situ sampling down to ~150 km (and later to ~120 km during deep dip campaigns) provides a means to collect thermosphere-ionosphere datasets below ~500 km (and down to the homopause) along the orbit tracks. These "along the track" profiles cannot be assumed to be vertical only, since variations in altitude are accompanied by variations in latitude, longitude and local time for each orbit. Since the MAVEN spacecraft precesses in latitude and local time (see Fig. 1 from Zurek et al. 2014, this issue), multiple orbits can be assembled and studied to extract trends separately in each of these independent variables. A detailed strategy will be developed to sample batches of orbits for which some of these parameters (e.g. local time) can be assumed to vary slowly. In addition, sorting/binning is needed to create 2-D maps of these key parameters for comparison to 3-D thermosphere-ionosphere model simulations (see Lillis et al. 2014).

5 Conclusions and Summary

5.1 MAVEN Measurements Will Be Used to Characterize the Reservoir That Regulates Escape

The Mars thermosphere-ionosphere-exosphere (TIE) system constitutes the atmospheric reservoir (i.e. available cold and hot planetary neutral and thermal ion species) that regulates present day escape processes from the planet. The characterization of this TIE system, including its spatial and temporal (e.g., solar cycle, seasonal, diurnal, episodic) variability is needed to determine present day escape rates. Without knowledge of the physics and chemistry creating this TIE region and driving its variations, it is not possible to constrain either the short term or long term histories of atmosphere escape from Mars.

MAVEN will make both in-situ and remote measurements of the state variables of the Martian TIE system. A full characterization of the thermosphere (∼100–250 km) and ionosphere (∼100–400 km) structure (and its variability) will be conducted with the collection of spacecraft in-situ measurements (NGIMS, LPW, STATIC) that systematically span most local times and latitudes, over a regular sampling of Mars seasons, and throughout the bottom half of the solar cycle. Such sampling will far surpass that available from existing datasets. In addition, remote measurements (IUVS) will provide a systematic mapping of the composition and structure of Mars neutral upper atmosphere and coronae (e.g. H, C, N, O), as well as probe lower altitudes. Such a detailed characterization is a necessary first step toward answering MAVEN's three main science questions. This information will be used to determine present day escape rates from Mars, and provide an estimate of integrated loss to space throughout Mars history.

5.2 How Will Models Be Used in Conjunction with MAVEN Data to Determine Atmospheric Escape Rates?

The application of numerical models to determine Martian escape rates is reviewed in detail by Lillis et al. (2014). In brief, MAVEN in-situ and remote measurements must be combined with numerical models to: (a) explicitly determine neutral escape rates using TIE measurements from many instruments, and (b) set measured ion escape rates in the context of the variable solar wind environment and TIE structure. Both these applications are essential to develop a proper understanding of the underlying drivers and processes regulating neutral and ion escape rates. Only then is it possible to proceed with these same numerical models and extrapolate backwards in time to address the time evolution of these escape processes and rates over Mars history.

References

M. Angelats i Coll, F. Forget, M.A. López-Valverde et al., Upper atmosphere of Mars up to 120 km: Mars Global Surveyor data analysis with the LMD general circulation model. J. Geophys. Res. **109**, E01011 (2004). doi:10.1029/2003JE002163

D.T. Baird, R. Tolson, S.W. Bougher, B. Steers, Zonal wind calculation from MGS Accelerometer and rate data. AIAA J. Spacecr. Rockets **44**(6), 1180–1187 (2007)

C.A. Barth, A.I.F. Stewart, S.W. Bougher et al., Aeronomy of the current martian atmosphere, in *Mars*, ed. by H.H. Kieffer, B.M. Jakosky, C.W. Snyder, M.S. Matthews (University of Arizona Press, Tucson, 1992), pp. 1054–1089

J.-L. Bertaux, E. Chassefiere, V.G. Kurt, Vensu EUV measurements of hydrogen and helium from Venera 11 and Venera 12. Adv. Space Res. **5**, 119–124 (1985)

J.-L. Bertaux, F. Leblanc, S. Perrier et al., Nightglow in the upper atmosphere of Mars and implications for atmospheric transport. Science **307**, 566–569 (2005a). doi:10.1126/science.1106957
J.-L. Bertaux, F. Leblanc, O. Witasse et al., Discovery of an aurora on Mars. Nature **435**, 790–794 (2005b)
S.W. Bougher, Comparative thermospheres: Venus and Mars. Adv. Space Res. **15**(4), 21–25 (1995)
S.W. Bougher, Coupled MGCM-MTGCM Mars thermosphere simulations and resulting data products in support of the MAVEN mission. *JPL/CDP report*, pp. 1–9, 6 August 2012 (2012)
S.W. Bougher, M.J. Alexander, H.G. Mayr, Upper atmosphere dynamics: global circulation and gravity waves, in *Venus II: Geology, Geophysics, Atmosphere, and Solar Wind Environment*, ed. by S.W. Bougher, D.M. Hunten, R.J. Phillips (University of Arizona Press, Tucson, 1997), pp. 259–291
S.W. Bougher, G. Keating, R. Zurek et al., Mars global surveyor aerobraking: Atmospheric trends and model interpretation. Adv. Space Res. **23**, 1887–1897 (1999a). doi:10.1016/S0273-1177(99)00272-0
S.W. Bougher, S. Engel, R.G. Roble, B. Foster, Comparative terrestrial planet thermospheres 2. Solar cycle variation of global structure and winds at equinox. J. Geophys. Res. **104**, 16591–16611 (1999b). doi:10.1029/1998JE001019
S.W. Bougher, S. Engel, R.G. Roble, B. Foster, Comparative terrestrial planet thermospheres 3. Solar cycle variation of global structure and winds at solstices. J. Geophys. Res. **105**, 17669–17692 (2000). doi:10.1029/1999JE001232
S.W. Bougher, R.G. Roble, T.J. Fuller-Rowell, Simulations of the upper atmospheres of the terrestrial planets, in *Atmospheres in the Solar System, Comparative Aeronomy*, ed. by M. Mendillo, A.F. Nagy, J.H. Waite Jr. AGU Monograph, vol. 130 (American Geophysical Union, Washington, 2002), pp. 261–288
S.W. Bougher, S. Engel, D.P. Hinson, J.R. Murphy, MGS Radio Science electron density profiles: Interannual variability and implications for the martian neutral atmosphere. J. Geophys. Res. **109**, E03010 (2004). doi:10.1029/2003JE002154
S.W. Bougher, J.M. Bell, J.R. Murphy et al., Polar warming in the Mars thermosphere: Seasonal variations owing to changing isolation and dust distributions. Geophys. Res. Lett. **33**, L02203 (2006). doi:10.1029/2005GL024059
S.W. Bougher, P.-L. Blelly, M. Combi et al., Neutral upper atmosphere and ionosphere modeling. Space Sci. Rev. **139**, 107–141 (2008). doi:10.1007/s11214-008-9401-9
S.W. Bougher, A. Valeille, M.R. Combi, V. Tenishev, Solar cycle and seasonal variability of the martian thermosphere-ionosphere and associated impacts upon atmospheric escape. SAE Technical Paper #2009-01-2386, SAE International (2009a)
S.W. Bougher, T.M. McDunn, K.A. Zoldak, J.M. Forbes, Solar cycle variability of Mars dayside exospheric temperatures: Model evaluation of underlying thermal balances. Geophys. Res. Lett. **36**, L05201 (2009b). doi:10.1029/2008GL036376
S.W. Bougher, A. Ridley, D. Pawlowski et al., Development and validation of the ground-to-exosphere Mars GITM code: solar cycle and seasonal variations of the upper atmosphere, in *The Fourth International Workshop on the Mars Atmosphere: Modeling and Observations*, Paris, France (2011a)
S.W. Bougher, D.J. Pawlowski, J.R. Murphy, Toward an understanding of the time-dependent responses of the martian upper atmosphere to dust storm events, in *2011 Fall AGU Meeting*, San Francisco, California (2011b)
S.W. Bougher, D.A. Brain, J.L. Fox, F. Gonzalez-Galindo, C. Simon-Wedlund, P.G. Withers, Upper neutral atmosphere and ionosphere, in *Mars Book II* (Cambridge University Press, Cambridge, 2014), accepted, Chap. 14
D.A. Brain, S. Barabash, S.W. Bougher, F. Duru, B.M. Jakosky, R. Modolo, Solar wind interaction and atmospheric escape, in *Mars Book II* (Cambridge University Press, Cambridge, 2014), accepted, Chap. 15
P.C. Chamberlain, T.N. Woods, F.G. Eparvier, Flare irradiance spectral model (FISM): Daily component algorithms and results. Space Weather **6**(S05), 001 (2008). doi:10.1029/2007SW000372
S. Chapman, The absorption and dissociation of ionizing effect of monochromatic radiation in an atmosphere on a rotating Earth. Proc. Phys. Soc. **43**, 26–45 (1931)
E. Chassefiere, F. Leblanc, Mars atmospheric escape and evolution: Interaction with the solar wind. Planet. Space Sci. **52**, 1039–1058 (2004)
J.Y. Chaufray, R. Modolo, F. Leblanc, G. Chanteur, R.E. Johnson, J.G. Luhmann, Mars solar wind interaction: Formation of the Martian corona and atmospheric loss to space. J. Geophys. Res. **112**, E09009 (2007). doi:10.1029/2007JE002915
J.Y. Chaufray, F. Leblanc, E. Quémerais, J.L. Bertaux, Martian oxygen density at the exobase deduced from O I 130.4-nm observations by spectroscopy for the investigation of the characteristics of the atmosphere of Mars on Mars Express. J. Geophys. Res. **114**, E02006 (2009)
F. Cipriani, F. Leblanc, J.J. Berthelier, Martian corona: Nonthermal sources of hot heavy species. J. Geophys. Res. **112**, E07001 (2007). doi:10.1029/2006JE002818
J.E.P. Connerney et al., The Magnetometer (MAG) (2014). http://lasp.colorado.edu/home/maven/science/instrument-package/mag

D.H. Crider, D.A. Brain, M.A. Acuña, D. Vignes, C. Mazelle, C. Bertucci, Mars global surveyor observations of solar wind magnetic field draping around Mars. Space Sci. Rev. **111**(1), 203–221 (2004). doi:10.1023/B:SPAC.0000032714.66124.4e

Z. Dobe, A.F. Nagy, J.L. Fox, A theoretical study concerning the solar cycle dependence of the nightside ionosphere of Venus. J. Geophys. Res. **100**, 14507–14513 (1995)

C. Dong, S.W. Bougher, Y. Ma, G. Toth, A.F. Nagy, D. Najib, Solar wind interaction with Mars upper atmosphere: Results from the one-way coupling between the multi-fluid MHD model and the MTGCM model. Geophys. Res. Lett. **41**, 1–8 (2014). doi:10.1002/2014GL059515

F. Duru, D.A. Gurnett, D.D. Morgan, R. Modolo, A.F. Nagy, D. Najib, Electron densities in the upper ionosphere of Mars from the excitation of electron plasma oscillations. J. Geophys. Res. **113**, A07302 (2008). doi:10.1029/2008JA013073

F. Duru, D.A. Gurnett, R.A. Frahm, J.D. Winningham, D.D. Morgan, G.G. Howes, Steep transient density gradients in the Martian ionosphere similar to the ionopause at Venus. J. Geophys. Res. **114**(A), 12310 (2009). doi:10.1029/2009JA014711

F. Duru, D.A. Gurnett, J.D. Winningham, R. Frahm, R. Modolo, A plasma flow velocity boundary at Mars from the disappearance of electron plasma oscillations. Icarus **206**(1), 74–82 (2010). doi:10.1016/j.icarus.2009.04.012

S.L. England, R.J. Lillis, On the nature of the variability of the Martian thermospheric mass density: Results from the electron reflectometry with Mars Global Surveyor. J. Geophys. Res. **117**, E02008 (2012). doi:10.1029/2011JE003998

F.G. Eparvier et al., The extreme ultraviolet (EUV) monitor (2014). http://lasp.colorado.edu/home/maven/science/instrument-package/lpw/extreme-ultraviolet-euv-monitor

R.E. Ergun et al., The Langmuir probe and waves (LPW) instrument (2014). http://lasp.colorado.edu/home/maven/science/instrument-package/lpw

X. Fang, S.W. Bougher, et al., The importance of pickup oxygen ion precipitation to the Mars upper atmosphere under extreme solar wind conditions. Geophys. Res. Lett. **40** (2013). doi:10.1029/grl.50415.2013

P.D. Feldman et al., Rosetta-Alice observations of exospheric hydrogen and oxygen on Mars. Icarus **214**, 394–399 (2011)

M.O. Fillingim, L.M. Peticolas, R.J. Lillis et al., Model calculations of electron precipitation induced ionization patches on the nightside of Mars. Geophys. Res. Lett. **34**, L12101 (2007). doi:10.1029/2007GL029986

G. Fjeldbo, V.R. Eshleman, The atmosphere of Mars analyzed by integral inversion of the Mariner IV occultation data. Planet. Space Sci. **16**, 1035–1059 (1968)

J.M. Forbes, M.E. Hagan, Diurnal Kelvin wave in the atmosphere of Mars: Towards an understanding of "stationary" density structures observed by the MGS Accelerometer. Geophys. Res. Lett. **27**, 21 (2000). doi:10.1029/2000GL011850

J.M. Forbes, A.F.C. Bridger, S.W. Bougher et al., Nonmigrating tides in the thermosphere of Mars. J. Geophys. Res. **107**, 5113 (2002). doi:10.1029/2001JE001582

J.M. Forbes, F.G. Lemoine, S.L. Bruinsma et al., Solar flux variability of Mars' exosphere densities and temperatures. Geophys. Res. Lett. **35**, L01201 (2008). doi:10.1029/2007GL031904

F. Forget, F. Montmessin, J.-L. Bertaux et al., Density and temperatures of the upper martian atmosphere measured by stellar occultations with Mars Express SPICAM. J. Geophys. Res. **114**, E01004 (2009). doi:10.1029/2008JE003086

J.L. Fox, Morphology of the dayside ionosphere of Mars: Implication for ion outflows. J. Geophys. Res. **114**, E12005 (2009). doi:10.1029/2009JE003432

J.L. Fox, A.B. Hać, Photochemical escape of oxygen from Mars: A comparison of the exobase approximation to a Monte Carlo method. Icarus **204**, 527–544 (2009). doi:10.1016/j.icarus.2009.07.005

J.L. Fox, A.B. Hać, Isotope fractionation in the photochemical escape of O from Mars. Icarus **208**, 176–191 (2010). doi:10.1016/j.icarus.2010.01.019

J.L. Fox, A.J. Kliore, Ionosphere: solar cycle variations, in *Venus II: Geology, Geophysics, Atmosphere and Solar Wind Environment*, ed. by S.W. Bougher, D.M. Hunten, R.J. Phillips (University of Arizona Press, Tucson, 1997)

J.L. Fox, J.F. Brannon, H.S. Porter, Upper limits to the nightside ionosphere of Mars. Geophys. Res. Lett. **20**, 1339–1342 (1993)

J.L. Fox, P. Zhou, S.W. Bougher, The thermosphere/ionosphere of Mars at high and low solar activities. Adv. Space Res. **17**, (11)203–(11)218 (1996)

M. Fränz, E. Dubinin, E. Nielsen et al., Transterminator ion flow in the martian ionosphere. Planet. Space Sci. **58**, 1442–1454 (2010)

T. Fuller-Rowell, S.C. Solomon, Flares, coronal mass ejections, and atmospheric responses, in *Heliophysics—Space Storms and Radiation: Causes and Effects*, ed. by C.J. Schrijver, G.L. Siscoe (Cambridge University Press, Cambridge, 2010), pp. 321–357

F. González-Galindo, F. Forget, M.A. López-Valverde et al., A ground-to-exosphere martian general circulation model: 1. Seasonal, diurnal, and solar cycle variation of thermospheric temperatures. J. Geophys. Res. **114**, E04001 (2009). doi:10.1029/2008JE003246

G. Gronoff, C. Simon-Wedlund, C.J. Mertens et al., Computing uncertainties in ionosphere-airglow models. II. The martian airglow. J. Geophys. Res. **117**, A05309 (2012). doi:10.1029/2011JA017308

D.A. Gurnett, R.L. Huff, D.D. Morgan et al., An overview of radar soundings of the martian ionosphere from the Mars Express spacecraft. Adv. Space Res. **41**, 1335–1346 (2008)

S.A. Haider, K.K. Mahajan, E. Kallio, Mars ionosphere: A review of experimental results and modeling studies. Rev. Geophys. **49**, RG4001 (2011). doi:10.1029/2011RG000357

W.B. Hanson, G.P. Mantas, Viking electron temperature measurements—Evidence for a magnetic field in the martian ionosphere. J. Geophys. Res. **93**, 7538–7544 (1988)

W.B. Hanson, S. Sanatani, D.R. Zuccaro, The martian ionosphere as observed by the Viking retarding potential analyzers. J. Geophys. Res. **82**, 4351–4363 (1977)

J.S. Halekas et al., The solar wind ion analyzer for MAVEN. Space Sci. Rev. (2013, this issue). doi:10.1007/s11214-013-0029-z

D.P. Hinson, R.A. Simpson, J.D. Twicken et al., Initial results from radio occultation measurements with Mars Global Surveyor. J. Geophys. Res. **104**, 26997–27012 (1999)

R.R. Hodges, The rate of loss of water from Mars. Geophys. Res. Lett. **29**(3), 1038 (2002). doi:10.1029/2001GL013853

D.L. Huestis, T.G. Slanger, B.D. Sharpee, J.L. Fox, Chemical origins of the Mars ultraviolet dayglow. Faraday Discuss. **147**, 307–322 (2010)

B.M. Jakosky, MAVEN: A Mars Scout Phase A Concept Study Report. Version 2: No Cost Edited, 1–109 (2008)

B.M. Jakosky et al., The MAVEN mission to Mars: exploring Mars' climate history, in *6th Alfven Conference, Abstract, 7–11 July* (UCL, London, 2014)

W.T. Kasprzak, G.M. Keating, N.C. Hsu, A.I.F. Stewart, W.B. Colwell, S.W. Bougher, Solar activity behavior of the thermosphere, in *Venus II: Geology, Geophysics, Atmosphere, and Solar Wind Environment*, ed. by S.W. Bougher, D.M. Hunten, R.J. Phillips (University of Arizona Press, Tucson, 1997), pp. 225–257

G.M. Keating, S.W. Bougher, R.W. Zurek et al., The structure of the upper atmosphere of Mars: In situ accelerometer measurements from Mars Global Surveyor. Science **279**, 1672–1676 (1998)

G.M. Keating, M. Theriot, R. Tolson et al., Brief review on the results obtained with the MGS and Mars Odyssey 2001 accelerometer experiments, in *Mars Atmosphere: Modeling and Observations Workshop*, Granada, Spain (2003)

G.M. Keating, S.W. Bougher, M.E. Theriot et al., Atmospheric structure from Mars reconnaissance orbiter accelerometer measurements, in *Proceedings of European Planetary Science Congress*, Berlin, Germany (2006)

G.M. Keating, S.W. Bougher, M.E. Theriot, R.H. Tolson, Properties of the Mars upper atmosphere derived from accelerometer measurements, in *Proceedings of 37th COSPAR Scientific Assembly 2008 and 50th Anniversary*, Montreal, Canada (2008)

Y.H. Kim, S. Son, Y. Yi, J. Kim, A non-spherical model for the hot oxygen corona of Mars. J. Korean Astron. Soc. **34**, 25–29 (2001)

A.J. Kliore, D.L. Cain, G. Fjeldbo et al., The atmosphere of Mars from Mariner 9 radio occultation measurements. Icarus **17**, 484–516 (1972)

V.A. Krasnopolsky, Solar activity variations of thermospheric temperatures on Mars and a problem of CO in the lower atmosphere. Icarus **207**, 638–647 (2010)

V.A. Krasnopolsky, P.D. Feldman, Far ultraviolet spectrum of Mars. Icarus **160**, 86–94 (2002)

M.A. Krestyanikova, V.I. Shematovitch, Stochastic models of hot planetary and satellite coronas: A photochemical source of hot oxygen in the upper atmosphere of Mars. Sol. Syst. Res. **39**, 22–32 (2005)

T.P. Larson et al., The solar energetic particle (SEP) instrument (2014). http://lasp.colorado.edu/home/maven/science/instrument-package/sep

F. Leblanc, J.Y. Chaufray, J. Lilensten et al., Martian dayglow as seen by the SPICAM UV spectrograph on Mars Express. J. Geophys. Res. **111**(9) (2006). doi:10.1029/2005JE002664

C. Lee et al., Thermal tides in the Martian middle atmosphere as seen by the Mars Climate Sounder. J. Geophys. Res. **114**, E03005 (2009). doi:10.1029/2008JE003285

Y. Lee, M. Combi, V. Tenishev, S.W. Bougher, Hot carbon corona in Mars' upper thermosphere and exosphere: 1. Mechanisms and structure of the hot corona for low solar activity at Equinox. J. Geophys. Res. (2014). doi:10.1002/2013JE004552

R.J. Lillis, S.W. Bougher, F. González-Galindo et al., Four martian years of nightside upper thermospheric mass densities derived from electron reflectometry: Method extension and comparison with GCM simulations. J. Geophys. Res. **115**, E07014 (2010). doi:10.1029/2009JE003529

R.J. Lillis et al., Photochemical escape of the Martian atmosphere: looking forward to MAVEN, in *6th Alfven Conference, Abstract, 7–11 July* (UCL, London, 2014)
J. Liu, M.I. Richardson, R.J. Wilson, An assessment of the global, seasonal, and interannual spacecraft record of Martian climate in the thermal infrared. J. Geophys. Res. **108**(E8), 5089 (2003). doi:10.1029/2002JE001921
R. Lundin et al., A comet-like escape of ionospheric plasma from Mars. Geophys. Res. Lett. **35**, L18203 (2008). doi:10.1029/2008GL034811
Y. Ma, A.F. Nagy, Ion escape fluxes from Mars. Geophys. Res. Lett. **34**, L08201 (2007). doi:10.1029/2006GL029208
Y. Ma, A.F. Nagy, I.V. Sokolov, K.C. Hansen, Three-dimensional, multispecies, high spatial resolution MHD studies of the solar wind interaction with Mars. J. Geophys. Res. **109**, A07211 (2004). doi:10.1029/2003JA010367
Y.J. Ma, X. Fang, A.F. Nagy, C.T. Russell, G. Toth, Martian ionospheric responses to dynamic pressure enhancements in the solar wind. J. Geophys. Res. **119**, 1272–1286 (2014). doi:10.1002/2013JA019402
P.R. Mahaffy et al., Space Sci. Rev. (2014, this issue). doi:10.1007/s11214-014-0043-9
M. Matta, P. Withers, M. Mendillo, The composition of Mars' topside ionosphere: Effects of hydrogen. J. Geophys. Res. **118**, 1–13 (2013). doi:10.1002/jgra.50104
W. McClintock et al., The imaging ultraviolet spectrograph (IUVS) (2014). http://lasp.colorado.edu/home/maven/science/instrument-package/iuvs
T.L. McDunn, S.W. Bougher, J. Murphy et al., Simulating the density and thermal structure of the middle atmosphere (80–130 km) of Mars using the MGCM-MTGCM: A comparison with MEX/SPICAM observations. Icarus **206**, 5–17 (2010)
J. McFadden et al., The suprathermal and thermal ion composition (STATIC) instrument (2014). http://lasp.colorado.edu/home/maven/science/instrument-package/static
M. Mendillo, S. Smith, J. Wroten et al., Simultaneous ionospheric variability on Earth and Mars. J. Geophys. Res. **108**, 1432 (2003). doi:10.1029/2003JA009961
M. Mendillo, P. Withers, D. Hinson et al., Effects of solar flares on the ionosphere of Mars. Science **311**, 1135–1138 (2006)
M. Mendillo, A.G. Marusiak, P. Withers, D. Morgan, D. Gurnett, A new semi-empirical model of the peak electron density of the martian ionosphere. Geophys. Res. Lett. **40**, 5361–5365 (2013). doi:10.1002/2013GL057631
D.L. Mitchell, R.P. Lin, H. Rème, D.H. Crider, P.A. Cloutier, J.E.P. Connerney, M.H. Acuña, N.F. Ness, Oxygen Auger electrons observed in Mars' ionosphere. Geophys. Res. Lett. **27**(1), 1871–1874 (2000). doi:10.1029/1999GL010754
D.L. Mitchell, R.P. Lin, C. Mazelle et al., Probing Mars' crustal magnetic field and ionosphere with the MGS electron reflectometer. J. Geophys. Res. **106**, 23419–23428 (2001)
D.G. Mitchell et al., The Solar Wind Electron Analyzer (SWEA) (2014). http://lasp.colorado.edu/home/maven/science/instrument-package/swea
D.D. Morgan, D.A. Gurnett, D.L. Kirchner et al., Variation of the Martian ionospheric electron density from Mars Express radar soundings. J. Geophys. Res. **113**, A09303 (2008). doi:10.1029/2008JA013313
Y. Moudden, J.M. Forbes, Effects of vertically propagating thermal tides on the mean structure and dynamics of Mars' lower thermosphere. Geophys. Res. Lett. **35**, L23805 (2008). doi:10.1029/2008GL036086
Y. Moudden, J.M. Forbes, A new interpretation of Mars aerobraking variability: Planetary wave-tide interactions. J. Geophys. Res. **115**, E09005 (2010). doi:10.1029/2009JE003542
I.C.F. Müeller-Wodarg, D.F. Strobel, J.I. Moses et al., Neutral atmospheres. Space Sci. Rev. **139** (2008). doi:10.1007/s11214-008-9404-6
A.F. Nagy, T.E. Cravens, Hot oxygen atoms in the upper atmospheres of Venus and Mars. Geophys. Res. Lett. **15**(5), 433–435 (1988)
A.F. Nagy, T.E. Cravens, J.H. Lee, A.I.F. Stewart, Hot oxygen atoms in the upper atmosphere of Venus. Geophys. Res. Lett. **8**, 629–632 (1981)
D. Najib, A.F. Nagy, G. Toth, Y. Ma, Three-dimensional, multi-fluid, high spatial resolution MHD model studies of the solar wind interaction with Mars. J. Geophys. Res. **116**, A05204 (2011). doi:10.1029/2010JA016272
F. Němec, D.D. Morgan, D.A. Gurnett, F. Duru, Nightside ionosphere of Mars: Radar soundings by the Mars Express spacecraft. J. Geophys. Res. **115**, E12009 (2010). doi:10.1029/2010JE003663
F. Němec, D.D. Morgan, D.A. Gurnett, D.A. Brain, Areas of enhanced ionization in the deep nightside ionosphere of Mars. J. Geophys. Res. **116**, E06006 (2011). doi:10.1029/2011JE003804
E. Nielsen, M. Fraenz, H. Zou et al., Local plasma processes and enhanced electron densities in the lower ionosphere in magnetic cusp regions on Mars. Planet. Space Sci. **55**, 2164–2172 (2007)
A.O. Nier, M.B. McElroy, Composition and structure of Mars' upper atmosphere: Results from the Neutral Mass Spectrometers on Viking 1 and 2. J. Geophys. Res. **82**, 4341–4349 (1977)

M. Pätzold, S. Tellmann, B. Häusler et al., A sporadic third layer in the ionosphere of Mars. Science **310**, 837–839 (2005)
D.J. Pawlowski, S.W. Bougher, Comparative aeronomy: the effects of solar flares at Earth and Mars, in *Comparative Climatology of Terrestrial Planets Conference*, Boulder, Colorado (2012)
D.J. Pawlowski, S.W. Bougher, P. Chamberlain, Modeling the response of the martian upper atmosphere to solar flares, in *2011 Fall AGU Meeting*, San Francisco, California (2011)
L.J. Paxton, Pioneer Venus Orbiter ultraviolet spectrometer limb observations: Analysis and interpretation of the 166- and 156-nm data. J. Geophys. Res. **90**, 5089–5096 (1985)
T. Penz, I. Arshukova, N. Terada, H. Shinagawa, N.V. Erkaev, H.K. Biernat, H. Lammer, A comparison of magnetohydrodynamic instabilities at the Martian ionopause. Adv. Space Res. **36**(1), 2049–2056 (2005). doi:10.1016/j.asr.2004.11.039
A. Safaeinili, W. Kofman, J. Mouginot et al., Estimation of the total electron content of the martian ionosphere using radar sounder surface echoes. Geophys. Res. Lett. **34**, L23204 (2007). doi:10.1029/2007GL032154
R. Schunk, A. Nagy, *Ionospheres: Physics, Plasma Physics, and Chemistry*, 2nd edn. (Cambridge University Press, New York, 2009)
A. Seiff, D.B. Kirk, Structure of the atmosphere of Mars in summer at mid-latitudes. J. Geophys. Res. **82**, 4364–4378 (1977)
M.D. Smith, Interannual variability in TES atmospheric observations of Mars during 1999–2003. Icarus **167**, 148–165 (2004)
M.D. Smith, THEMIS observations of Mars aerosol optical depth from 2002–2008. Icarus **202**, 444–452 (2009)
M.D. Smith, S.W. Bougher, T. Encrenaz, F. Forget, A. Kleinbohl, Thermal structure and composition, in *Mars Book II* (Cambridge University Press, Cambridge, 2014), accepted, Chap. 4
A. Stewart, Mariner 6 and 7 ultraviolet spectrometer experiment: Implications of CO_2^+, CO and O airglow. J. Geophys. Res. **77**, 1 (1972). doi:10.1029/JA077i001p00054
A.I.F. Stewart, Revised time dependent model of the martian atmosphere for use in orbit lifetime and sustenance studies. LASP-JPL Internal Report, NQ-802429, Jet Propulsion Lab, Pasadena, California (1987)
A.I. Stewart, C.A. Barth, C.W. Hord, A.L. Lane, Mariner 9 ultraviolet spectrometer experiment: Structure of Mars's upper atmosphere. Icarus **17**, 469–474 (1972)
A.I. Stewart, M.J. Alexander, R.R. Meier et al., Atomic oxygen in the martian thermosphere. J. Geophys. Res. **97**, 91–102 (1992)
A. Stiepen, J.-C. Gerard, S. Bougher, F. Montmessin, B. Hubert, Mars thermospheric temperatures from CO Cameron and CO_2^+ dayglow observations from Mars Express. Icarus (2014, submitted)
D.J. Strickland, G.E. Thomas, P.R. Sparks, Mariner 6 and 7 ultraviolet spectrometer experiment: Analysis of the O I 1304- and 1356-Å emissions. J. Geophys. Res. **77**, 4052–4068 (1972)
D.J. Strickland, A.I. Stewart, C.A. Barth et al., Mariner 9 ultraviolet spectrometer experiment: Mars atomic oxygen 1304-Å emission. J. Geophys. Res. **78**, 4547–4559 (1973)
R.H. Tolson, G.M. Keating, G.J. Cancro et al., Application of accelerometer data to Mars Global Surveyor aerobraking operations. J. Spacecr. Rockets **36**(3), 323–329 (1999)
R.H. Tolson, A.M. Dwyer, J.L. Hanna et al., Application of accelerometer data to Mars aerobraking and atmospheric modeling. J. Spacecr. Rockets **42**(3), 435–443 (2005)
R.H. Tolson, G.M. Keating, R.W. Zurek et al., Application of accelerometer data to atmospheric modeling during Mars aerobraking operations. J. Spacecr. Rockets **44**(6), 1172–1179 (2007)
R.H. Tolson, E. Bemis, S. Hough et al., Atmospheric modeling using accelerometer data during Mars Reconnaissance Orbiter aerobraking operations. J. Spacecr. Rockets **45**(3), 511–518 (2008)
A. Valeille, M.R. Combi, S.W. Bougher et al., Three-dimensional study of Mars upper thermosphere/ionosphere and hot oxygen corona: 1. General description and results at equinox for solar low conditions. J. Geophys. Res. **114**, E11005 (2009a). doi:10.1029/2009JE003388
A. Valeille, M.R. Combi, S.W. Bougher et al., Three-dimensional study of Mars upper thermosphere/ionosphere and hot oxygen corona: 2. Solar cycle, seasonal variations and evolution over history. J. Geophys. Res. **114**, E11006 (2009b). doi:10.1029/2009JE003389
A. Valeille, M.R. Combi, V. Tenishev et al., A study of suprathermal oxygen atoms in Mars upper thermosphere and exosphere over the range of limiting conditions. Icarus **206**, 18–27 (2010a)
A. Valeille, S.W. Bougher, V. Tenishev, M.R. Combi, A.F. Nagy, Water loss and evolution of the upper atmosphere and exosphere over Martian history. Icarus **206**, 28–39 (2010b)
Y.-C. Wang, J.G. Luhmann, F. Leblanc, X. Fang, R.E. Johnson, Y. Ma, W.-H. Ip, L. Li, Modeling of the sputtering efficiency for Martian atmosphere, in *Abstract P23A-1907 Presented at 2012 Fall Meeting, AGU*, San Francisco, CA, 3–7 Dec. 2012 (2012)
R.J. Wilson, Evidence for non-migrating thermal tides in the Mars upper atmosphere from the Mars Global Surveyor Accelerometer Experiment. Geophys. Res. Lett. **29**(7) (2002). doi:10.1029/2001GL013975

P.G. Withers, Mars Gobal Surveyor and Mars Odyssey accelerometer observations of the martian upper atmosphere during aerobraking. Geophys. Res. Lett. **33**, L02201 (2006). doi:10.1029/2005GL024447
P.G. Withers, A review of observed variability in the dayside ionosphere of Mars. Adv. Space Res. **44**, 277–307 (2009)
P.G. Withers, R. Pratt, An observational study of the response of the upper atmosphere of Mars to lower atmospheric dust storms. Icarus **225**, 378–389 (2013)
P.G. Withers, S.W. Bougher, G.M. Keating, The effects of topographically controlled thermal tides in the martian upper atmosphere as seen by the MGS accelerometer. Icarus **164**, 14–32 (2003)
P.G. Withers, M. Mendillo, H. Risbeth et al., Ionospheric characteristics above martian crustal magnetic anomalies. Geophys. Res. Lett. **32**, L16204 (2005). doi:10.1029/2005GL023483
M. Yagi, F. Leblanc, J.Y. Chaufray, F. Gonzalez-Galindo, S. Hess, R. Modolo, Mars exospheric thermal and non-thermal components: Seasonal and local variations. Icarus **221**, 682–693 (2012)
M.H.G. Zhang, J.G. Luhmann, A.J. Kliore, J. Kim, A post-Pioneer Venus reassessment of the martian dayside ionosphere as observed by radio occultation methods. J. Geophys. Res. **95**, 14829–14839 (1990a)
M.H.G. Zhang, J.G. Luhmann, A.J. Kliore, An observational study of the nightside ionospheres of Mars and Venus with radio occultation methods. J. Geophys. Res. **95**, 17095–17102 (1990b)
R.W. Zurek et al., Application of MAVEN accelerometer and attitude control data to Mars atmospheric characterization. Space Sci. Rev. (2014, this issue). doi:10.1007/s11214-014-0053-7